

1 **Structural and Biochemical Characterization of Rm3, a SubClass B3 Metallo-**  
2  **$\beta$ -Lactamase Identified from a Functional Metagenomic Study**

3 Ramya Salimraj<sup>1</sup>, Lihong Zhang<sup>2,3\*</sup>, Philip Hinchliffe<sup>1</sup>, Elizabeth M. H. Wellington<sup>2</sup>, Jürgen  
4 Brem<sup>4</sup>, Christopher J. Schofield<sup>4</sup>, William H. Gaze<sup>2,3\*</sup> and James Spencer<sup>1#</sup>

5 <sup>1</sup>School of Cellular and Molecular Medicine, University of Bristol Medical Sciences Building,  
6 University Walk, Bristol BS8 1TD, United Kingdom.

7 <sup>2</sup>School of Life Sciences, University of Warwick, Coventry CV4 7AL, United Kingdom

8 <sup>3</sup>European Centre for Environment and Human Health, University of Exeter Medical School,  
9 Knowledge Spa, Royal Cornwall Hospital, Truro, Cornwall TR1 3HD, UK

10 <sup>4</sup>Department of Chemistry, University of Oxford, 12 Mansfield Road, Oxford, OX1 3TA, United  
11 Kingdom

12 \* present address

13 #Correspondence and reprints.

14 Mailing address for James Spencer: School of Cellular and Molecular Medicine, University of  
15 Bristol, Biomedical Sciences Building, University Walk, Bristol BS8 1TD, United Kingdom.

16 Phone: (44) (0) 117 331 2084.

17 Fax: (44) (0) 117 331 2091.

18 E-mail: Jim.Spencer@bristol.ac.uk

19 Running Title: Characterization of Rm3 metallo- $\beta$ -lactamase

20 **Abstract**

21  $\beta$ -Lactamase production increasingly threatens the effectiveness of  $\beta$ -lactams, which remain a  
22 mainstay of antimicrobial chemotherapy. New activities emerge both through mutation of  
23 previously known  $\beta$ -lactamases and mobilization from environmental reservoirs. The spread of  
24 metallo- $\beta$ -lactamases (MBLs) represents a particular challenge through their typically broad  
25 spectrum activities, encompassing carbapenems in addition to other  $\beta$ -lactam classes.  
26 Increasingly, genomic and metagenomic studies reveal distribution of putative MBLs in the  
27 environment, but in most cases their activity against clinically relevant  $\beta$ -lactams, and hence the  
28 extent to which they can be considered a resistance reservoir, remains uncharacterized. Here we  
29 characterize the product of one such gene, *bla<sub>Rm3</sub>*, identified through functional metagenomic  
30 sampling of an environment with high biocide exposure. *bla<sub>Rm3</sub>* encodes a subclass B3 MBL that,  
31 when expressed in recombinant *E. coli*, is exported to the bacterial periplasm and hydrolyzes  
32 clinically used penicillins, cephalosporins, and carbapenems with an efficiency limited by high  
33  $K_M$  values. An Rm3 crystal structure reveals the MBL superfamily  $\alpha\beta/\beta\alpha$  fold, which more  
34 closely resembles mobilized B3 MBLs (AIM-1, SMB-1) than other chromosomal enzymes (L1  
35 or FEZ-1). A binuclear zinc site sits in a deep channel that is in part defined by a relatively  
36 extended N-terminus. Structural comparisons suggest that the steric constraints imposed by the  
37 N-terminus may limit  $\beta$ -lactam affinity. Sequence comparisons identify Rm3-like MBLs in  
38 numerous other environmental samples and species. Our data suggest that Rm3 like enzymes  
39 represent a distinct group of B3 MBLs with a wide distribution and can be considered as an  
40 environmental reservoir of  $\beta$ -lactam resistance.

41 **Introduction**

42 The continued efficacy of  $\beta$ -lactam antibiotics is threatened by the dissemination of  $\beta$ -  
43 lactamases, hydrolytic enzymes that inactivate these important drugs by cleavage of the scissile  
44  $\beta$ -lactam amide bond (1). In the 70 years since  $\beta$ -lactams were first introduced to the clinic,  
45 repeated mobilizations of  $\beta$ -lactamase genes from a variety of bacterial sources have led to their  
46 rapid propagation in opportunistic Gram-negative pathogens such as the Enterobacteriaceae and  
47 non-fermenting species including *Pseudomonas aeruginosa* and *Acinetobacter baumannii* (2).  
48 Notably, some of the most successful  $\beta$ -lactamases, in particular the CTX-M extended-spectrum  
49  $\beta$ -lactamase (ESBL) associated with resistance to third-generation cephalosporins such as  
50 cefotaxime, and which is now distributed worldwide (3), find their origins in environmental  
51 organisms, illustrating how transfer of antibiotic resistance genes from environmental to  
52 pathogenic species can have profound clinical consequences (4). In the case of CTX-M enzymes  
53 it is now accepted that these originated in *Kluyvera* spp. (5, 6), a Gram-negative rod bacterium  
54 that is found in both the human intestinal microbiome and the wider natural environment (7).

55  $\beta$ -Lactamases are divided, primarily on the basis of amino acid sequence, into four main classes  
56 (8). Of these, three (classes A, C and D) are active site nucleophilic serine enzymes (SBLs) and  
57 the remaining class, B, zinc metalloenzymes that are structurally and mechanistically unrelated  
58 to the SBLs. The metallo- $\beta$ -lactamases (MBLs) are themselves divided into a further three  
59 groups (B1, B2 and B3) on the basis of sequence differences that are manifest as variations in the  
60 number (1 or 2) of zinc ions required for full activity, and in structural differences that include  
61 variations in co-ordination of the active site zinc ions (9, 10). MBLs are a growing clinical  
62 concern as they effectively hydrolyze all  $\beta$ -lactam classes excepting the monobactams and

## Characterization of Rm3 Metallo- $\beta$ -Lactamase

63 escape the action of SBL inhibitors (11) that are at (clavulanate, tazobactam) or close to  
64 (avibactam, relebactam) the clinic. B1 MBLs such as the NDM (12) and VIM (13) enzymes are  
65 now encountered with increasing frequency on mobile genetic elements in organisms such as  
66 *Escherichia coli*, *Klebsiella pneumoniae*, *P. aeruginosa* and *A. baumannii*.

67 While B3 family members such as AIM-1 (14) and SMB-1 (15) have been identified on mobile  
68 genetic elements, the majority of these enzymes are chromosomal. However, in addition to their  
69 presence in opportunist pathogens such as *Stenotrophomonas maltophilia* (16) and  
70 *Elizabethkingia meningosepticum* (17), the B3 MBLs also have a very wide distribution in  
71 environmental organisms and sequences. Compared to the B1 enzymes, the B3 MBLs are less  
72 well studied, display a greater degree of structural and sequence diversity and are more closely  
73 related to other branches of the wider metallo-hydrolase superfamily to which the MBLs belong  
74 (18). Investigations of B3 MBLs from environmental sources will thus expand our understanding  
75 of activity and structure within this group of enzymes and provide insights into the nature and  
76 extent to which MBLs in the environment provide a reservoir of resistance determinants to the  
77 most clinically important  $\beta$ -lactam antibiotics. Furthermore, identifying how the distribution of  
78 such sequences changes in response to human activity (i.e. exposure to antimicrobials within the  
79 environment) can also provide evidence of the effect of human activity upon the environmental  
80 resistance reservoir (19).

81 Technological advances have transformed our ability to sample and identify antibiotic resistance  
82 genes in the natural environment. In particular, combining sequence-based (metagenomics) with  
83 functional (construction and analysis of large libraries) methodologies can both establish the  
84 prevalence and distribution of putative resistance genes and identify those that confer a  
85 resistance phenotype, i.e. that are able to alter antibiotic susceptibility in a model organism (e.g.

## Characterization of Rm3 Metallo- $\beta$ -Lactamase

86 *E. coli*) (20-22). This study provides a biochemical and structural characterization of a B3 MBL,  
87 Rm3, that was identified by application of this functional metagenomics approach to study the  
88 distribution of resistance to third-generation cephalosporins in environmental sources selected on  
89 the basis of differing degrees of human impact. (Full details of the identification of Rm3 will be  
90 presented elsewhere). The *bla*<sub>Rm3</sub> gene (GenBank accession KF485393.2) was isolated from a  
91 metagenomic library derived from soil from a reed bed used to bioremediate effluent from a  
92 textile mill with high usage of quaternary ammonium compounds (QACs). Screening of this  
93 library identified *bla*<sub>Rm3</sub> as one of a number of novel  $\beta$ -lactamase genes able to decrease  
94 susceptibility of recombinant *E. coli* to third generation cephalosporins.

95 The Rm3 amino acid sequence (Figure 1) most closely resembles other putative B3 MBLs from  
96 environmental bacteria, in particular sequences from the soil bacteria *Janthinobacterium* (e.g.  
97 GenBank KKO63914.1; 89 % sequence identity (23)) and *Solimonas* (e.g. NCBI accession  
98 WP\_020650668.1; 56 % identity) *spp.* Rm3 also resembles (54 % sequence identity) a novel B3  
99 MBL, LRA-8, identified from a metagenomics study of the Tanana river in Central Alaska (20)  
100 (Figure 1), and a related sequence (GenBank AIA12579.1; 56 % identity) identified from a  
101 grassland soil sample from Minnesota, U.S.A., as part of a functional metagenomics study of  
102 environmental antibiotic resistance genes (24). Of biochemically characterized B3 MBLs, Rm3  
103 shares the highest sequence identity with THIN-B (25) (49%) and is between 43% (SMB-1) (15)  
104 and 27% (BJP-1) (26) identical to enzymes of known structure. On this basis, (Figures 1,2), Rm3  
105 can be considered as being representative of a group of uncharacterized novel B3 MBLs that  
106 appear to be widely distributed within the environmental microbiome. Here we present the  
107 biochemical and structural characterization of recombinant Rm3.

108

109 **Materials and Methods**

110 **Identification of *bla*<sub>Rm3</sub>**

111 Full details of the identification of Rm3 will be presented elsewhere. Briefly, core samples were  
112 obtained from reed beds used for remediation of effluent from a textile mill in Yorkshire, U.K.,  
113 (27) and total DNA was purified as previously described (21). A metagenomic library was  
114 generated by cloning purified DNA fragments into plasmid pCF430 (28) and transforming into  
115 *E. coli* strain EC100 (Epicentre, Madison WI, U.S.A.) by electroporation. Recombinants were  
116 passaged over 10-20 generations and clones resistant to third generation cephalosporins selected  
117 by plating on ceftazidime (1  $\mu$ g / ml). Putative resistance genes were identified by sequencing  
118 positive clones, and their contribution to the resistance phenotype confirmed by inactivation  
119 using transposon mutagenesis (EZ-Tn5 kit, Epicentre) allowing for selection by loss of  
120 phenotype (21).

121

122 **Minimal Inhibitory Concentration (MIC) Determination for Metagenomic Clones**

123 Minimal inhibitory concentration (MIC) values for metagenomic clones were determined by agar  
124 dilution on Iso-sensi Test Agar (Oxoid) with an inoculum of  $10^5$  colony forming units (cfu) per  
125 spot (29).

126

127 **Recombinant Rm3 Expression and Purification**

128 The complete Rm3 open reading frame (including the putative periplasmic export sequence) was  
129 amplified from metagenomic clone RM3 by PCR with primers RM3F

## Characterization of Rm3 Metallo- $\beta$ -Lactamase

130 (AAGGCATATGATGTCCTCACACCACCACGCGCG) and RM3R2(AATGGGATCCTTAC  
131 TGCTGTTTTTCCTGGT) with proof-reading Pfu DNA polymerase. The product was ligated  
132 into the T7 expression vector pET26b (30) using the Nde1 and BamH1 restriction sites and the  
133 integrity of the resulting plasmid pLHZRM3 confirmed by DNA sequencing. *E. coli*  
134 ArcticExpress (DE3) competent cells (Agilent, Stockport, U.K.) transformed with pLHZRM3  
135 were grown (Power Broth (Athena Enzyme Systems, Baltimore, MD, U.S.A.); 30° C; 160 rpm  
136 shaking) to  $OD_{600nm} \approx 0.6$  and expression induced overnight (1 mM isopropyl- $\beta$ -D-  
137 thiogalactopyranoside (Melford Laboratories, Ipswich, U.K.); 13° C). Cells were harvested by  
138 centrifugation (7 205 g; 30 mins; 4° C) and lysed in a Constant Systems (Daventry, U.K.) cell  
139 disruptor (25 000 psi). Debris was removed by centrifugation (38 724 g, 1 h) and the supernatant  
140 exchanged into buffer A (50 mM potassium phosphate pH 7.0, 1 M ammonium sulfate) by  
141 extensive dialysis using a 3 000 Da cut-off membrane (Medicell International, London, U.K.).

142 Protein for crystallography was purified by the following method. 20 ml of the dialysate was  
143 loaded on a 1 ml Phenyl FF HS column (GE Healthcare Life Sciences, Little Chalfont, U.K.) and  
144 the column washed consecutively with buffer B (buffer A plus 10 mM  $MgCl_2$ , 5 mM ATP, 50  
145 mM KCl) and buffer A prior to elution on a gradient of 0 – 50 % buffer C (50 mM potassium  
146 phosphate pH 7.0). Rm3-containing fractions were identified by SDS-PAGE (31) and  
147 concentrated to a volume of ~2 ml by centrifugal ultrafiltration using an Amicon concentrator  
148 with a 3 000 Da molecular weight cut off (Millipore, Watford, U.K.). Protein was loaded onto a  
149 300 ml Superdex S75 size exclusion column (GE Healthcare) and eluted with a flow rate of 1 ml  
150 / min in buffer D (20 mM Tris pH 7.5, 200 mM NaCl). Rm3-containing fractions were pooled  
151 and concentrated as above.

## Characterization of Rm3 Metallo- $\beta$ -Lactamase

152 For enzyme kinetic experiments Rm3 was purified by a modified version of the above protocol  
153 where recombinant protein was produced in *E. coli* SoluBL21 cells (AMS Biotechnology,  
154 Abingdon, U.K.) that were grown overnight in Autoinduction Terrific Broth (Formedium,  
155 Hunstanton, U.K.) at 25° C. The hydrophobic interaction chromatography step utilized a 40 ml  
156 Phenyl FF HS column, omitted the ATP wash and eluted bound protein on a 0 – 100 % buffer C  
157 gradient; and size exclusion chromatography utilized a 120 ml HiLoad 16/60 Superdex 75 pg  
158 column (GE Healthcare).

159

### 160 **Verification of Recombinant Rm3 by Mass Spectrometry**

161 ESI mass analyses were acquired (as described (32)) in the positive ion mode using a Waters  
162 (Elstree, U.K.) LCT Premier instrument equipped with a TOF analyzer. An LCT Premier mass  
163 spectrometer (Waters) was coupled to an Agilent 1100 Series HPLC using a Chromolith®  
164 FastGradient RP-18 endcapped column equipped with a 50-2 HPLC column, made of  
165 monolithic silica (C18, 2 x 50 mm, macropores with 1.6  $\mu$ m diameter, Merck (Beeston, U.K.)).  
166 The instrument was connected to a CTC-autosampler inlet system. A multi-step gradient over  
167 10 min was run (solvent A 94.9% H<sub>2</sub>O/5% CH<sub>3</sub>CN/0.1% formic acid, solvent B 99.9%  
168 CH<sub>3</sub>CN/0.1% formic acid; 0-1 min 5% B for equilibration, followed by a linear gradient to  
169 100% B over 4 min, then 100% B for an additional 3 min, followed by a linear gradient over 2  
170 min back to 5% B to re-equilibrate the column) to separate the protein samples at flow rates of  
171 0.4 ml / min for the first 5 min and then 1.0 ml / min for the remaining time. The electrospray  
172 ionization source used a capillary voltage of 3.2 kV and cone voltage of 25 V. Nitrogen was used  
173 as the nebulizer and desolvation gas at a flow rate of 600 l/h. Protein typically eluted as a peak



174 between 3 and 5 min under these conditions. Calculated masses were obtained using the ExPasy  
175 ProtParam tool (<http://web.expasy.org/protparam/> (33)).

176

### 177 **Steady-State Kinetics of $\beta$ -Lactam Hydrolysis by Recombinant Rm3**

178 Hydrolysis of selected  $\beta$ -lactams by recombinant Rm3 was investigated under steady-state  
179 conditions. The buffer was 50 mM HEPES, pH 7.0, supplemented with 100  $\mu$ M ZnCl<sub>2</sub> and 100  
180  $\mu$ g/ml BSA and the protein concentration was 10 nM. Measurements used either a Polarstar  
181 Omega plate reader (BMG LabTech, Aylesbury, U.K.) or, for complete hydrolysis curves, a  
182 Lamda 35 spectrophotometer (Perkin-Elmer, Seer Green, U.K.). Extinction coefficients and  
183 wavelengths used (34) were: -775 M<sup>-1</sup> cm<sup>-1</sup> at 235 nm (penicillin G); -820 M<sup>-1</sup> cm<sup>-1</sup> at 235 nm  
184 (ampicillin); -7700 M<sup>-1</sup> cm<sup>-1</sup> at 260 nm (cefoxitin); -9000 M<sup>-1</sup> cm<sup>-1</sup> at 260 nm (ceftazidime); -  
185 7500 M<sup>-1</sup> cm<sup>-1</sup>-at 260 nm (cefotaxime); - 6500 M<sup>-1</sup> cm<sup>-1</sup> at 300 nm (meropenem); - 9000 M<sup>-1</sup> cm<sup>-1</sup>  
186 at 300 nm (imipenem); and -700 M<sup>-1</sup> cm<sup>-1</sup> at 320 nm (aztreonam).

187 Data were analyzed by fitting to the Michaelis-Menten equation:

$$188 \quad V = k_{cat} * [E] * [S] / (K_M + [S])$$

189 Where V is the measured initial velocity at substrate concentration [S] and [E] is the  
190 concentration of enzyme. Where high apparent  $K_M$  values precluded data collection under the  
191 conditions required to achieve saturation of hydrolysis rate, the value of  $k_{cat}/K_M$  was measured by  
192 fitting progress curves (absorbance versus time) for a complete hydrolysis reaction to the  
193 exponential:

$$194 \quad A_t = A_\infty + (A_0 - A_\infty) * e^{-kt}$$

195 where  $A_t$  is the absorbance at time  $t$  and  $A_0$  the initial and  $A_\infty$  the final absorbance. The observed  
196 first-order rate constant is then  $k = (k_{cat}/K_M)*[E]$  (35). Curve fitting was undertaken using Prism  
197 (GraphPad, La Jolla, CA, U.S.A.).

198

### 199 **Rm3 Crystallization and Structure Determination**

200 Purified Rm3 protein in buffer D was concentrated to  $\sim 13$  mg / ml by ultracentrifugation as  
201 above and supplemented with  $100 \mu\text{M}$   $\text{ZnCl}_2$  and  $5 \text{ mM}$  Tris(2-carboxyethyl)phosphine (TCEP)  
202 hydrochloride (Fisher Scientific). Initial crystallization hits were obtained from commercial  
203 sparse matrix screening kits (Molecular Dimensions (Newmarket, U.K.) Proplex (36)) using a  
204 Phoenix crystallization robot (Art Robbins Instruments, Sunnyvale, CA, U.S.A.) to set  $100 \text{ nl}$   
205 plus  $100 \text{ nl}$  sitting drops in 96-well MRC plates (Molecular Dimensions) using a reservoir  
206 volume of  $100 \mu\text{l}$ . Conditions were optimized using  $1 \mu\text{l}$  plus  $1 \mu\text{l}$  hanging drops in 24-well XRL  
207 plates (Molecular Dimensions) with  $500 \mu\text{L}$  reservoir volume. Diffraction data were collected  
208 from a single crystal grown in a hanging drop from  $14\%$  w/v PEG 8000,  $0.1 \text{ M}$  Tris pH 8,  $0.15$   
209  $\text{M}$  LiCl. All crystallization experiments were carried out at  $18^\circ\text{C}$ .

210 The Rm3 crystal was cryoprotected for  $\sim 30$  seconds by exposure to reservoir solution  
211 supplemented with  $25\%$  ethylene glycol, mounted in a SPINE standard pin (Molecular  
212 Dimensions) and flash frozen in liquid nitrogen. Diffraction data were collected on beamline I04  
213 of the Diamond Light Source (DLS), U.K., using a Pilatus 6M-F detector.  $934$  images of  $0.15^\circ$   
214 oscillation (exposure  $0.15 \text{ s}$  per image;  $20\%$  beam intensity) were collected at a wavelength of  
215  $0.9795 \text{ \AA}$ . Diffraction data were integrated using XDS (37), the space group was identified using  
216 Pointless (38) and data were scaled and merged using Aimless (38) as implemented in the Xia2

## Characterization of Rm3 Metallo- $\beta$ -Lactamase

217 pipeline (39). The structure was solved by molecular replacement using Phaser (40) with  
218 Chainsaw (41) used to create a search model based upon *S. maltophilia* L1 (chain A of PDB  
219 2QDT (42)) by pruning side chains of non-identical amino acids to their C $\gamma$  atoms. Models were  
220 built in Coot (43) and refinement carried out using Refmac 5 (44). Final refinement and model  
221 validation (MolProbity (45)) took place in Phenix (46).

222 Coordinates and structure factors have been deposited in the Protein Data Bank  
223 ([www.rcsb.org/pdb](http://www.rcsb.org/pdb)) with accession no. 5IQK.

224

## 225 **Results and Discussion**

### 226 **Identification of Rm3 as a Subclass B3 Metallo- $\beta$ -Lactamase**

227 *bla<sub>Rm3</sub>* was identified by selecting ceftazidime resistant clones from a metagenomic library  
228 constructed from DNA purified from samples originating from a reed bed used to bioremediate  
229 effluent from a textile mill with high usage of quaternary ammonium compounds (QACs). QACs  
230 are disinfective agents with wide industrial application, and have been implicated in the selection  
231 of co- and cross-resistance to a variety of antibiotic classes, including  $\beta$ -lactams (47, 48). *bla<sub>Rm3</sub>*  
232 was situated on an 8 kb DNA fragment (metagenomic clone RM3; GenBank accession  
233 KF485393.2) that exerted variable effects upon susceptibility to  $\beta$ -lactam antibiotics but that  
234 resulted in a 16-fold elevation of the MIC of *E. coli* EC100 to CAZ (ceftazidime) compared to  
235 vector-only control (Table 1). This effect was abolished by insertional inactivation of *bla<sub>Rm3</sub>* by  
236 transposition (data not shown). The amino acid sequence of the *bla<sub>Rm3</sub>* encoded protein, Rm3,  
237 showed properties (presence of a His116-Xaa-His118-Xaa-Asp120-His121 sequence motif and  
238 similarity to previously characterized enzymes) characteristic of a subclass B3 MBL (Figure 1).

239

### 240 **Expression and Kinetic Characterization of Recombinant Rm3**

241 The *bla<sub>Rm3</sub>* gene encodes a 302 residue polypeptide that includes an N-terminal leader peptide of  
242 23 residues that was identified by SignalP (49) as a periplasmic export sequence. The complete  
243 Rm3 open reading frame, including the putative export sequence, was expressed in either *E. coli*  
244 ArcticExpress or SoluBL21 and was purified to apparent homogeneity by hydrophobic  
245 interaction and size exclusion chromatography. Quadrupole time-of-flight (QTOF) mass  
246 spectrometry under denaturing conditions gave a mass of 29 805 Da for the purified protein,

## Characterization of Rm3 Metallo- $\beta$ -Lactamase

247 consistent with a predicted mass of 29 808.5 Da for the Rm3 fragment resulting from removal of  
248 the predicted precursor polypeptide after residue 23. Thus these data confirm that the leader  
249 peptide is removed from recombinant Rm3 by post-translational processing in *E. coli*, and  
250 strongly indicate that, as is the case for other  $\beta$ -lactamases of Gram-negative bacteria, the protein  
251 is exported to the bacterial periplasm.

252 Steady-state kinetic experiments indicate that Rm3 is able to hydrolyze a range of penicillin,  
253 cephalosporin, and carbapenem antibiotics with varying degrees of efficiency (Table 2). Notably,  
254 it was possible to obtain accurate  $K_M$  estimates for only two substrates, meropenem and  
255 ampicillin, of the eight that were evaluated. For the other substrates tested it proved difficult to  
256 saturate the Michaelis-Menten (i.e. rate versus substrate concentration) plots, indicating high  $K_M$   
257 values and likely low affinity. For these substrates, values for catalytic efficiency ( $k_{cat}/K_M$ ) only  
258 are reported. Overall catalytic efficiencies approaching  $10^5 \text{ M}^{-1} \text{ s}^{-1}$  are achieved for substrates  
259 from all classes excepting the monobactam aztreonam, against which Rm3, as is the case for  
260 other MBLs, shows no hydrolytic activity. These data show Rm3, in common with most other  
261 B3 MBLs, to be an enzyme with a broad spectrum of activity. The relatively low catalytic  
262 efficiencies that are achieved by Rm3, compared to other characterized B3 MBLs where values  
263 for  $k_{cat}/K_M$  in excess of  $10^7 \text{ M}^{-1} \text{ s}^{-1}$  have been reported for some favorable enzyme:substrate  
264 combinations (e.g. AIM-1-catalyzed imipenem hydrolysis (14)), arise primarily from the  
265 relatively high  $K_M$  values. For all substrates tested  $K_M$  values were  $10^{-4} \text{ M}$  or above, contrasting  
266 with most other B3 MBLs where for more favored substrates  $K_M$  values of  $10^{-5} \text{ M}$  or better are  
267 obtained. Some other enzymes from environmental sources, such as *J. lividum* BJP-1 (26),  
268 *Erwinia caratovora* CAR-1 (50) and *Caulobacter crescentus* CAU-1 (51), are also notable for  
269 comparably high  $K_M$  values across the range of  $\beta$ -lactams. However, Rm3 is distinguished from

270 many of these by an apparent lack of discrimination against oxyiminocephalosporins (e.g.  
271 ceftazidime) or 7- $\alpha$ -methoxy cephalosporins (e.g. cefoxitin) that are poor substrates for the B3  
272 enzymes CAR-1 and CAU-1, respectively.  $k_{cat}/K_M$  values for hydrolysis of these substrates by  
273 Rm3 are in line with those for other  $\beta$ -lactams tested.

274

### 275 **Crystal Structure of Rm3**

276 Rm3 crystallized in space group  $P2_1$  with two molecules in the asymmetric unit. A single 1.75 Å  
277 resolution dataset was collected at the Diamond Light Source synchrotron radiation facility and  
278 phases and an initial electron density map calculated by molecular replacement. Data collection  
279 and refinement statistics are given in Table 3. The final structure contains 268 (chain A) and 269  
280 (chain B) residues, with electron density not observed for the 10 (chain A) or 9 (chain B) N-  
281 terminal amino acids, or for the C-terminal glutamine residue of either polypeptide chain. We  
282 note that the N-terminus of processed Rm3 is formed by a proline-rich sequence (QTPAPATPP)  
283 that is likely to be unstructured in solution. 96.6 % of total residues are in the most favored  
284 regions of the Ramachandran plot, with no residues classed as outliers. The overall structure  
285 (Figure 3) is that of the MBL superfamily, comprising an  $\alpha\beta / \beta\alpha$  fold in which the N- and C-  
286 terminal halves of the protein form central seven- and five-stranded  $\beta$ -sheets, respectively, that  
287 are flanked by  $\alpha$ -helices. The interface of these two sheets provides the location for the active  
288 site. The active site environment is defined by three loop regions that connect elements of  
289 secondary structure: residues 150 – 164 (loop 1) connecting helix  $\alpha_4$  and strand  $\beta_7$ ; residues 192  
290 – 201 that connect strands  $\beta_9$  and  $\beta_{10}$  and residues 222 – 239 (loop 2) connecting strand  $\beta_{11}$  and  
291 helix  $\alpha_5$ . (The BBL numbering scheme (52) is used throughout this manuscript).

## Characterization of Rm3 Metallo- $\beta$ -Lactamase

292 The presence of disulfide bonds also serves to define the overall architecture of the Rm3  
293 structure. The processed Rm3 polypeptide contains a total of 6 Cys residues, of which two  
294 (residues 256 and 290) form a disulfide bond between helices  $\alpha 5$  and  $\alpha 7$  that is common to all  
295 B3 MBLs of known structure excepting BJP-1 (53). In chain A of the current structure a second  
296 disulfide between Cys208 and Cys213 constrains the short loop between strands  $\beta 10$  and  $\beta 11$ .  
297 However, in chain B this disulfide bond is not present, Cys208 and Cys213 are reduced and a  
298 zinc ion is positioned between them. This zinc ion is also coordinated by His246 and Glu249 of  
299 an adjacent chain and thus occupies a site that is formed at the interface of two Rm3 monomers  
300 in adjacent asymmetric units in the crystal. The final pair of Cys residues (positions 32 and 35)  
301 also contribute to a further zinc site at the interface between the two Rm3 molecules present in  
302 the crystallographic asymmetric unit, in which zinc co-ordination is completed by His158 of the  
303 opposing chain, and by a crystallographic water molecule. However, as Rm3 eluted from the size  
304 exclusion chromatography column at a volume consistent with a molecular weight of  
305 approximately 30 000 Da (data not shown), indicating that the protein is likely to exist as a  
306 monomer in solution, we consider both of these interface sites to be crystallization artefacts that  
307 are unlikely to exert a physiological function.

308 Inspection of difference electron density maps from the early stages of refinement  
309 unambiguously identified the presence of two metal ions in the Rm3 active site. These were  
310 refined as zinc ions, based upon the presence of excess zinc in the crystallization experiment and  
311 the absence of other metal ions in the crystal as adjudged by the lack of additional peaks in an X-  
312 ray fluorescence excitation spectrum collected at the synchrotron beamline (data not shown).  
313 Both sites were refined to 100 % occupancy with B-factors similar to those of the adjacent  
314 protein atoms (Table 3). Consistent with assignment of Rm3 as a member of the B3 MBL

## Characterization of Rm3 Metallo- $\beta$ -Lactamase

315 subfamily, the two zinc ions respectively occupy the two binding sites that are defined by  
316 conserved residues of the MBL superfamily; i.e. a tri-histidine (Zn1) site formed by His116,  
317 His118 and His196 and an Asp – His – His (Zn2) site formed by Asp120, His121 and His263  
318 (Figure 4). In both subunits the two zinc ions lie approximately 3.5 Å apart (distances 3.46 Å and  
319 3.51 Å in chains A and B, respectively) and are connected by a “bridging” water molecule  
320 (Wat1, likely to exist as an hydroxide ion (54)) that is positioned asymmetrically with respect to  
321 the two metal ions and lies closer to Zn1 (1.81 - 1.90 Å) than to Zn2 (2.04 - 2.11 Å). Metal co-  
322 ordination is completed by a second water molecule (Wat2) that lies closer to Zn2 but also co-  
323 ordinates Zn1 (Wat2 – Zn1 distances 2.57 and 2.68 Å in chains A and B, respectively), and can  
324 thus also be considered to bridge the two metal ions. In consequence both Rm3 metal ions are  
325 five co-ordinated.

326 Five co-ordinate metal ion systems can be described using the structural parameter  $\tau$  ( $\tau = (\beta -$   
327  $\alpha)/60$ ) to discriminate between trigonal ( $\tau = 1$ ) and square ( $\tau = 0$ ) pyramidal geometries (55). For  
328 the Rm3 Zn1 site the two angles  $\alpha$  and  $\beta$  that represent distortion from square to trigonal  
329 bipyramidal co-ordination can be defined as His116 – Zn1 – His196 (103.5°) and Wat2 – Zn1 –  
330 His118 (167.4°), respectively (56), yielding a value for  $\tau$  of 1.07 and indicating that co-  
331 ordination is best described as trigonal bipyramidal. For the Zn2 site  $\alpha$  and  $\beta$  are defined as Wat1  
332 – Zn2 – His263 (127.4°) and Wat2 – Zn2 – Asp120 (155.9°), respectively (57), giving  $\tau = 0.475$   
333 and co-ordination geometry as intermediate between trigonal bi- and square pyramidal. In chain  
334 B Wat2 is less well defined by the experimental electron density but occupies a similar position,  
335 with values for  $\tau$  of 0.97 for the Zn1, and 0.41 for the Zn2, sites. Thus zinc co-ordination is  
336 similar in both Rm3 molecules.



337

### 338 **Comparison with Other B3 MBL Structures**

339 PDBeFold (58) was used to generate superpositions of chain B of Rm3 with five other B3 MBLs  
340 of known crystal structure: L1 (pdb 1SML (59), RMSD 1.47 Å over 240 C $\alpha$  atoms), FEZ-1 (pdb  
341 1K07 (60). RMSD 1.65 Å over 254 C $\alpha$  atoms), BJP-1 (pdb 3LVZ (53), RMSD 1.73 Å over 251  
342 C $\alpha$  atoms), AIM-1 (pdb 4AWY (61), RMSD 1.04 Å over 247 C $\alpha$  atoms) and SMB-1 (pdb 3VPE  
343 (57), RMSD 0.87 Å over 245 C $\alpha$  atoms). Thus, the Rm3 structure most closely resembles those  
344 of AIM-1 and SMB-1, consistent with the closer sequence relationship to these enzymes than to  
345 other structurally characterized B3 MBLs. Superposition of the B3 MBL structures (Figure 5)  
346 identifies three regions where there is variation between the various structures - the extreme N-  
347 terminus, the loop connecting helix  $\alpha$ 4 and strand  $\beta$ 7 (sometimes termed loop1) and that  
348 connecting strand  $\beta$ 11 and helix  $\alpha$ 5 (loop2 (57)). Together these three regions substantially  
349 define the active site groove in B3 MBLs. Notably, the N-terminal region of Rm3 is poorly  
350 defined in the crystal structure, with no electron density evident for the proline-rich sequence  
351 (QTPAPATPP) that forms the N-terminus of the processed polypeptide after cleavage of the  
352 signal peptide. However, unlike the AIM-1 and SMB-1 structures, where a turn preceding the  
353 conserved Trp41 forces relatively short N-termini away from the active site, in Rm3 Trp41 is  
354 part of an  $\alpha$ -helix ( $\alpha$ 1, Figure 3) that defines one wall of a deeper active site groove (Figure 5).  
355 Thus, in this regard Rm3 more closely resembles BJP-1, where an extended helical N-terminus  
356 creates an active site that is much narrower than those of other B3 MBLs of known structure.

357 Loop1 (residues 150 – 164) of B3 MBLs also contributes substantially to the active site  
358 architecture. Hydrophobic residues (Phe156 and Ile162) in loop1 of L1 were proposed to

## Characterization of Rm3 Metallo- $\beta$ -Lactamase

359 participate in binding of substrate (59), but subsequent directed mutagenesis investigations of L1  
360 (62) and FEZ-1 (63) did not identify these individual positions as essential to activity. However,  
361 rapid kinetic experiments (64) demonstrate that this loop can adjust its position during turnover  
362 of  $\beta$ -lactams by the L1 enzyme, indicating that the structure as a whole may have some  
363 mechanistic role. In addition, both AIM-1 and SMB-1 feature a Gln at position 157, where  
364 models of bound cephalosporin substrates suggest that it may interact with the carboxylate group  
365 at C7/C8 formed on hydrolysis of the  $\beta$ -lactam amide (57, 61). In Rm3 Gln157 is present, as part  
366 of a DPQ motif that is also found in SMB-1, AIM-1 and THIN-B, and the organization of loop1  
367 closely resembles that found in AIM-1 and SMB-1 (Figure 5). By way of contrast, loop1 in the  
368 L1, FEZ-1 and BJP-1 structures adopts a more “open” conformation than is the case here.

369 Loop2 (residues 224 - 230) is the third region of variability between B3 MBL structures. In  
370 common with AIM-1 and SMB-1, loop2 of Rm3 is longer by two residues than its equivalent in  
371 other B3 enzymes, with the apex of this loop extending away from the active site. In L1 and  
372 FEZ-1, residues such as Asn225 (FEZ-1) and Tyr228 (both enzymes) on loop2 are proposed to  
373 contribute to  $\beta$ -lactam hydrolysis through interaction with the C7/C8 carboxylate group of  
374 hydrolyzed species (see above) (59, 60, 62). Consistent with the presence of Gln157 on loop1  
375 (see above) which could act as a functional replacement for these residues, the equivalent  
376 positions of Rm3 loop2 are occupied by amino acids (Val and Pro) that are unable to replicate  
377 these proposed interactions, and the conformation of loop2 is also incompatible with a  
378 contribution to  $\beta$ -lactam binding and/or hydrolysis. Loop2 of BJP-1 also differs from the  
379 equivalent regions of L1 and FEZ-1, but in this case it is positioned in a more “closed”  
380 conformation nearer to the zinc center. Taken together, these comparisons indicate that, in both  
381 the overall fold, and the specific architecture of variable regions (loops 1 and 2) adjacent to the

382 active site, the Rm3 structure more closely resembles that of the mobile B3 enzymes AIM-1 and  
383 SMB-1 than it does the chromosomal B3 MBLs L1, FEZ-1 and BJP-1.

384 In contrast to these clear differences in overall structure between different B3 MBLs, comparison  
385 of the respective active sites indicates that the principal features of the Rm3 metal center are  
386 common between all structurally characterized B3 MBLs. Specifically, all B3 MBLs of known  
387 structure feature a binuclear zinc center with a five co-ordinate ion in the Zn2 site and geometry  
388 intermediate between trigonal bi- and square pyramidal, and (for structures that do not contain  
389 bound ligands) the zinc – zinc distance (3.46 Å and 3.51 Å in Rm3 chains A and B, respectively  
390 (see above)) varies between 3.40 and 3.58 Å (for structures determined at resolutions between  
391 1.40 Å and 1.80 Å, compared to a resolution of 1.75 Å for the structure of Rm3 presented here).  
392 With respect to other B3 enzymes, the main difference in the Rm3 active site is the positioning  
393 of the Wat2 water molecule (Figure 4b, c), which is notably closer to both Zn1 (distances 2.57 Å  
394 and 2.68 Å in Rm3 chains A and B, respectively) and Wat1 (2.33 Å and 1.96 Å) than is the case  
395 in e.g L1 (Wat2 – Zn1 and Wat2 – Wat1 distances 2.80 Å and 3.04 Å for pdb 1SML).

396

### 397 **Implications of Rm3 Structure for Activity**

398 Despite much effort, the precise mode of binding of  $\beta$ -lactams to the active site of B3 MBLs  
399 remains incompletely understood. In fact only one crystal structure has so far been determined  
400 for a B3 MBL complexed with antibiotic, that of L1 bound to the hydrolysis product of the  
401 oxacephem moxalactam (65); docking and quantum mechanics/molecular mechanics (QM/MM)  
402 approaches have been used to investigate interactions of AIM-1 with hydrolyzed cefoxitin (61).  
403 We therefore used superposition of the Rm3 and L1:moxalactam structures to consider possible

## Characterization of Rm3 Metallo- $\beta$ -Lactamase

404 interactions of hydrolyzed moxalactam with Rm3 (Figure 6a, b) in an effort to investigate  
405 determinants of  $\beta$ -lactamase activity, and the basis for the high  $K_M$  values that are observed for  
406  $\beta$ -lactam hydrolysis by Rm3.

407 Consistent with the ability of Rm3 to hydrolyze most classes of  $\beta$ -lactam, these comparisons  
408 imply that the enzyme can replicate many of the interactions with substrates made by L1 or  
409 AIM-1. In addition to interactions involving the two metal ions (Zn1 with the C7/C8  
410 carbonyl/carboxylate of the  $\beta$ -lactam amide, and Zn2 with the C3/C4 carboxylate of the second  
411 ring), the Rm3 active site contains conserved residues at positions previously implicated in  $\beta$ -  
412 lactam binding. In particular, Ser221, a residue that is highly conserved in B3 MBLs, and  
413 Asn223 (Ser or Thr in most other B3 enzymes) are well positioned to contact the C3/C4  
414 carboxylate of bound  $\beta$ -lactam. Notably, in the Rm3 crystal structure the anticipated positions  
415 adopted by the  $\beta$ -lactam carboxylate oxygen atoms are occupied by Wat2 and by a second water  
416 molecule (Wat3) positioned between the Ser221 and Asn223 side chains. As noted earlier, and as  
417 has been proposed for AIM-1 (61) and SMB-1 (57), the Gln157 side chain is positioned to  
418 contact the C7/C8 carboxylate generated by  $\beta$ -lactam hydrolysis. Furthermore, the conserved  
419 Trp41 side chain is able to make hydrophobic interactions with the  $\beta$ -lactam core. Rm3 is thus  
420 able to make productive interactions with the core components common across the different  
421 classes of  $\beta$ -lactam.

422 Given this apparent availability of productive modes of substrate binding, we then considered  
423 why Rm3 hydrolyzes  $\beta$ -lactams with relatively low efficiency. Inspection of molecular surfaces  
424 in the vicinity of the active site (Figure 6c, d) indicates that, compared to other B3 enzymes in  
425 which the active site sits in a relatively shallow groove, the Rm3 active site is positioned at the

426 bottom of a much deeper channel that runs across one side of the structure. Notably, the extended  
427 N-terminus forms one wall of this cleft in the region that would be expected to form the binding  
428 site for the C6/C7 (R1) substituent of  $\beta$ -lactams, either requiring substrates to adopt specific  
429 conformations on binding to avoid steric clashes, or necessitating significant conformational  
430 changes of the enzyme to render the active site more accessible to  $\beta$ -lactams, particularly those  
431 such as later generation cephalosporins (e.g. ceftazidime) with bulky C7 substituents.  
432 Interestingly, for the B3 MBL BJP-1, where in the unliganded enzyme the active site is occluded  
433 by the extended N-terminal  $\alpha$ -helix, the crystal structure of a complex with a 4-  
434 nitrobenzenesulfonamide inhibitor showed that inhibitor binding involved displacement of this  
435 entire helix from its position in the native structure in order to make the active site accessible  
436 (53). We thus propose that the high  $K_M$  values for Rm3-catalyzed hydrolysis of  $\beta$ -lactams arise  
437 in large part from the steric constraints upon substrate binding that are imposed by the extended  
438 N-terminus. It is possible that the additional proline-rich N-terminal sequence, comprising a  
439 further 10 amino acids that could not be modeled in our final crystal structure, could impose  
440 further restrictions upon substrate binding.

441

#### 442 **Concluding Remarks**

443 The increasing availability of sequence information from genomic and metagenomics projects  
444 has begun to establish the extent to which antibiotic resistance genes are distributed in the wider  
445 environment. It is now clear that MBLs, and the B3 subclass in particular, are frequently present  
446 on the chromosomes of environmental organisms that include, but are not limited to, opportunist  
447 human pathogens such as *S. maltophilia* or *E. meningosepticum*. Accumulating evidence shows

## Characterization of Rm3 Metallo- $\beta$ -Lactamase

448 that the antibiotic era has been characterized by repeated instances of the mobilization of  
449 resistance determinants from environmental species, such as *Kluyvera* or *Shewanella* spp., into  
450 clinically significant pathogens, and their subsequent global dissemination on multiresistance  
451 plasmids. It is also becoming apparent that exposure to detergents and biocides, as well as  
452 antibiotics, may also be implicated in the mobilization of resistance genes, and co-selection of  
453 multiresistance elements. In this work we describe the properties of the product of a novel  
454 resistance gene, *bla<sub>Rm3</sub>*, that was identified from an environment with high levels of biocide  
455 exposure.

456 *bla<sub>Rm3</sub>* encodes a B3 MBL that is active against most  $\beta$ -lactam classes *in vitro* and is able to  
457 reduce the cephalosporin susceptibility of recombinant *E. coli*, thus replicating characteristics of  
458 enzymes of clinical importance. Sequence-based phylogeny indicates that Rm3 is representative  
459 of a distinct clade of B3 MBLs that differs from the L1 and FEZ-1/GOB groups (Figure 2). It is  
460 likely that, given their occurrence in environmental samples from sites that differ greatly in their  
461 geographical location and level of human impact, these enzymes have a wide distribution in the  
462 environment. With increasing use of broad-spectrum  $\beta$ -lactams, and the associated increase in  
463 selection pressure, there is thus considerable potential for future mobilization of MBLs of this  
464 type into the clinic. The structure of Rm3 demonstrates an overall resemblance to the mobilized  
465 AIM-1 and SMB-1 enzymes, and provides a basis both for the  $\beta$ -lactamase activity of Rm3 and  
466 the limited efficiency with which it hydrolyzes most substrates. However, the architecture of the  
467 active site that is created by the extended N-terminus distinguishes Rm3 from other B3 MBLs  
468 that have been studied so far, suggesting both that (as has been suggested for other B3 MBLs  
469 (50))  $\beta$ -lactams may not necessarily be the natural substrates for these enzymes, and that there is

## Characterization of Rm3 Metallo- $\beta$ -Lactamase

470 capacity for  $\beta$ -lactamase activity to be improved by mutation. Future experiments will  
471 investigate these possibilities.

472 **Funding Information**

473 R.S., J.S., J.B. and C.J.S. are supported by the U.K. Medical Research Council (U.K.-Canada  
474 Team Grant G1100135) and P.H. and J.S. by the National Institute of Allergy and Infectious  
475 Diseases of the U.S. National Institutes of Health under award number R01AI100560. LZ, WHG  
476 and EMHW were supported by NERC NE/E004482/1 and a European Regional Development  
477 Fund, grant no. 500020. The content is solely the responsibility of the authors and does not  
478 necessarily represent the official views of the National Institutes of Health.

479 **Acknowledgements.**

480 We thank Diamond Light Source for access to beamline I04 (proposal number MX313) that  
481 contributed to the results presented here.

482



483 **References**

- 484 1. **Fisher JF, Meroueh SO, Mobashery S.** 2005. Bacterial resistance to  $\beta$ -lactam  
485 antibiotics: compelling opportunism, compelling opportunity. *Chem Rev* **105**:395-424.
- 486 2. **Bush K.** 2013. Proliferation and significance of clinically relevant  $\beta$ -lactamases. *Ann N*  
487 *Y Acad Sci* **1277**:84-90.
- 488 3. **D'Andrea MM, Arena F, Pallecchi L, Rossolini GM.** 2013. CTX-M-type  $\beta$ -  
489 lactamases: a successful story of antibiotic resistance. *Int J Med Microbiol* **303**:305-317.
- 490 4. **Wellington EM, Boxall AB, Cross P, Feil EJ, Gaze WH, Hawkey PM, Johnson-**  
491 **Rollings AS, Jones DL, Lee NM, Otten W, Thomas CM, Williams AP.** 2013. The role  
492 of the natural environment in the emergence of antibiotic resistance in Gram-negative  
493 bacteria. *Lancet Infect Dis* **13**:155-165.
- 494 5. **Humeniuk C, Arlet G, Gautier V, Grimont P, Labia R, Philippon A.** 2002.  $\beta$ -  
495 lactamases of *Kluyvera ascorbata*, probable progenitors of some plasmid-encoded CTX-  
496 M types. *Antimicrob Agents Chemother* **46**:3045-3049.
- 497 6. **Poirel L, Kampfer P, Nordmann P.** 2002. Chromosome-encoded Ambler class A  $\beta$ -  
498 lactamase of *Kluyvera georgiana*, a probable progenitor of a subgroup of CTX-M  
499 extended-spectrum  $\beta$ -lactamases. *Antimicrob Agents Chemother* **46**:4038-4040.
- 500 7. **Sarria JC, Vidal AM, Kimbrough RC, 3rd.** 2001. Infections caused by *Kluyvera*  
501 species in humans. *Clin Infect Dis* **33**:E69-74.
- 502 8. **Ambler RP.** 1980. The structure of  $\beta$ -lactamases. *Philos Trans R Soc Lond B Biol Sci*  
503 **289**:321-331.
- 504 9. **Palzkill T.** 2013. Metallo- $\beta$ -lactamase structure and function. *Ann N Y Acad Sci*  
505 **1277**:91-104.

- 506 10. **Crowder MW, Spencer J, Vila AJ.** 2006. Metallo- $\beta$ -lactamases: novel weaponry for  
507 antibiotic resistance in bacteria. *Acc Chem Res* **39**:721-728.
- 508 11. **Drawz SM, Bonomo RA.** 2010. Three decades of  $\beta$ -lactamase inhibitors. *Clin Microbiol*  
509 *Rev* **23**:160-201.
- 510 12. **Dortet L, Poirel L, Nordmann P.** 2014. Worldwide dissemination of the NDM-type  
511 carbapenemases in Gram-negative bacteria. *Biomed Res Int* **2014**:249856.
- 512 13. **Papagiannitsis CC, Izdebski R, Baraniak A, Fiett J, Herda M, Hrabak J, Derde LP,**  
513 **Bonten MJ, Carmeli Y, Goossens H, Hryniewicz W, Brun-Buisson C, Gniadkowski**  
514 **M, Mosar Wp WP, groups WPs, Mosar Wp WP, groups WPs.** 2015. Survey of  
515 metallo- $\beta$ -lactamase-producing Enterobacteriaceae colonizing patients in European ICUs  
516 and rehabilitation units, 2008-11. *J Antimicrob Chemother* **70**:1981-1988.
- 517 14. **Yong D, Toleman MA, Bell J, Ritchie B, Pratt R, Ryley H, Walsh TR.** 2012. Genetic  
518 and biochemical characterization of an acquired subgroup B3 metallo- $\beta$ -lactamase gene,  
519 *bla<sub>AIM-1</sub>*, and its unique genetic context in *Pseudomonas aeruginosa* from Australia.  
520 *Antimicrob Agents Chemother* **56**:6154-6159.
- 521 15. **Wachino J, Yoshida H, Yamane K, Suzuki S, Matsui M, Yamagishi T, Tsutsui A,**  
522 **Konda T, Shibayama K, Arakawa Y.** 2011. SMB-1, a novel subclass B3 metallo- $\beta$ -  
523 lactamase, associated with ISCR1 and a class 1 integron, from a carbapenem-resistant  
524 *Serratia marcescens* clinical isolate. *Antimicrob Agents Chemother* **55**:5143-5149.
- 525 16. **Bicknell R, Emanuel EL, Gagnon J, Waley SG.** 1985. The production and molecular  
526 properties of the zinc  $\beta$ -lactamase of *Pseudomonas maltophilia* IID 1275. *Biochem J*  
527 **229**:791-797.

- 528 17. **Bellais S, Aubert D, Naas T, Nordmann P.** 2000. Molecular and biochemical  
529 heterogeneity of class B carbapenem-hydrolyzing  $\beta$ -lactamases in *Chryseobacterium*  
530 *meningosepticum*. Antimicrob Agents Chemother **44**:1878-1886.
- 531 18. **Bebrone C.** 2007. Metallo- $\beta$ -lactamases (classification, activity, genetic organization,  
532 structure, zinc coordination) and their superfamily. Biochem Pharmacol **74**:1686-1701.
- 533 19. **Gaze WH, Krone SM, Larsson DG, Li XZ, Robinson JA, Simonet P, Smalla K,**  
534 **Timinouni M, Topp E, Wellington EM, Wright GD, Zhu YG.** 2013. Influence of  
535 humans on evolution and mobilization of environmental antibiotic resistome. Emerg  
536 Infect Dis **19**.
- 537 20. **Allen HK, Moe LA, Rodbumrer J, Gaarder A, Handelsman J.** 2009. Functional  
538 metagenomics reveals diverse  $\beta$ -lactamases in a remote Alaskan soil. ISME J **3**:243-251.
- 539 21. **Amos GC, Zhang L, Hawkey PM, Gaze WH, Wellington EM.** 2014. Functional  
540 metagenomic analysis reveals rivers are a reservoir for diverse antibiotic resistance genes.  
541 Vet Microbiol **171**:441-447.
- 542 22. **Torres-Cortes G, Millan V, Ramirez-Saad HC, Nisa-Martinez R, Toro N, Martinez-**  
543 **Abarca F.** 2011. Characterization of novel antibiotic resistance genes identified by  
544 functional metagenomics on soil samples. Environ Microbiol **13**:1101-1114.
- 545 23. **Shoemaker WR, Muscarella ME, Lennon JT.** 2015. Genome Sequence of the Soil  
546 Bacterium *Janthinobacterium* sp. KBS0711. Genome Announc **3**.
- 547 24. **Forsberg KJ, Patel S, Gibson MK, Lauber CL, Knight R, Fierer N, Dantas G.** 2014.  
548 Bacterial phylogeny structures soil resistomes across habitats. Nature **509**:612-616.

- 549 25. **Docquier JD, Lopizzo T, Liberatori S, Prenna M, Thaller MC, Frere JM, Rossolini**  
550 **GM.** 2004. Biochemical characterization of the THIN-B metallo- $\beta$ -lactamase of  
551 *Janthinobacterium lividum*. *Antimicrob Agents Chemother* **48**:4778-4783.
- 552 26. **Stoczko M, Frere JM, Rossolini GM, Docquier JD.** 2006. Postgenomic scan of  
553 metallo- $\beta$ -lactamase homologues in rhizobacteria: identification and characterization of  
554 BJP-1, a subclass B3 ortholog from *Bradyrhizobium japonicum*. *Antimicrob Agents*  
555 *Chemother* **50**:1973-1981.
- 556 27. **Gaze WH, Abdousslam N, Hawkey PM, Wellington EM.** 2005. Incidence of class 1  
557 integrons in a quaternary ammonium compound-polluted environment. *Antimicrob*  
558 *Agents Chemother* **49**:1802-1807.
- 559 28. **Newman JR, Fuqua C.** 1999. Broad-host-range expression vectors that carry the L-  
560 arabinose-inducible *Escherichia coli* araBAD promoter and the araC regulator. *Gene*  
561 **227**:197-203.
- 562 29. **Andrews JM.** 2001. Determination of minimum inhibitory concentrations. *J Antimicrob*  
563 *Chemother* **48**, **Supplement 1**:5-16.
- 564 30. **Studier FW, Rosenberg AH, Dunn JJ, Dubendorff JW.** 1990. Use of T7 RNA  
565 polymerase to direct expression of cloned genes. *Methods Enzymol* **185**:60-89.
- 566 31. **Laemmli UK.** 1970. Cleavage of structural proteins during the assembly of the head of  
567 bacteriophage T4. *Nature* **227**:680-685.
- 568 32. **Brem J, Struwe WB, Rydzik AM, Tarhonskaya H, Pfeffer I, Flashman E, van**  
569 **Berkel SS, Spencer J, Claridge TD, McDonough MA, Benesch JL, Schofield CJ.**  
570 2015. Studying the active-site loop movement of the Sao Paulo metallo- $\beta$ -lactamase-1.  
571 *Chem Sci* **6**:956-963.

- 572 33. **Wilkins MR, Gasteiger E, Bairoch A, Sanchez JC, Williams KL, Appel RD,**  
573 **Hochstrasser DF.** 1999. Protein identification and analysis tools in the ExPASy server.  
574 *Methods Mol Biol* **112**:531-552.
- 575 34. **Laraki N, Franceschini N, Rossolini GM, Santucci P, Meunier C, de Pauw E,**  
576 **Amicosante G, Frere JM, Galleni M.** 1999. Biochemical characterization of the  
577 *Pseudomonas aeruginosa* 101/1477 metallo- $\beta$ -lactamase IMP-1 produced by *Escherichia*  
578 *coli*. *Antimicrob Agents Chemother* **43**:902-906.
- 579 35. **Toth M, Vakulenko V, Antunes NT, Frase H, Vakulenko SB.** 2012. Class A  
580 carbapenemase FPH-1 from *Francisella philomiragia*. *Antimicrob Agents Chemother*  
581 **56**:2852-2857.
- 582 36. **Radaev S, Li S, Sun PD.** 2006. A survey of protein-protein complex crystallizations.  
583 *Acta Crystallogr D Biol Crystallogr* **62**:605-612.
- 584 37. **Kabsch W.** 2010. XDS. *Acta Crystallogr D Biol Crystallogr* **66**:125-132.
- 585 38. **Evans PR.** 2011. An introduction to data reduction: space-group determination, scaling  
586 and intensity statistics. *Acta Crystallogr D Biol Crystallogr* **67**:282-292.
- 587 39. **Winter G.** 2010. xia2: an expert system for macromolecular crystallography data  
588 reduction. *Journal of Applied Crystallography* **43**:186-190.
- 589 40. **McCoy AJ, Grosse-Kunstleve RW, Adams PD, Winn MD, Storoni LC, Read RJ.**  
590 2007. Phaser crystallographic software. *J Appl Cryst* **40**:658-674.
- 591 41. **Stein N.** 2008. CHAINSAW: a program for mutating pdb files used as templates in  
592 molecular replacement. *Journal of Applied Crystallography* **41**:641-643.
- 593 42. **Lienard BM, Garau G, Horsfall L, Karsisiotis AI, Damblon C, Lassaux P,**  
594 **Papamicael C, Roberts GC, Galleni M, Dideberg O, Frere JM, Schofield CJ.** 2008.

- 595 Structural basis for the broad-spectrum inhibition of metallo- $\beta$ -lactamases by thiols. *Org*  
596 *Biomol Chem* **6**:2282-2294.
- 597 43. **Emsley P, Lohkamp B, Scott WG, Cowtan K.** 2010. Features and development of  
598 Coot. *Acta Crystallogr D Biol Crystallogr* **66**:486-501.
- 599 44. **Murshudov GN, Vagin AA, Dodson EJ.** 1997. Refinement of Macromolecular  
600 Structures by the Maximum-Likelihood Method. *Acta Crystallogr D Biol Crystallogr*  
601 **53**:240-255.
- 602 45. **Chen VB, Arendall WB, 3rd, Headd JJ, Keedy DA, Immormino RM, Kapral GJ,**  
603 **Murray LW, Richardson JS, Richardson DC.** 2010. MolProbity: all-atom structure  
604 validation for macromolecular crystallography. *Acta Crystallogr D Biol Crystallogr*  
605 **66**:12-21.
- 606 46. **Adams PD, Afonine PV, Bunkoczi G, Chen VB, Davis IW, Echols N, Headd JJ,**  
607 **Hung LW, Kapral GJ, Grosse-Kunstleve RW, McCoy AJ, Moriarty NW, Oeffner R,**  
608 **Read RJ, Richardson DC, Richardson JS, Terwilliger TC, Zwart PH.** 2010.  
609 PHENIX: a comprehensive Python-based system for macromolecular structure solution.  
610 *Acta Crystallogr D Biol Crystallogr* **66**:213-221.
- 611 47. **Pal C, Bengtsson-Palme J, Kristiansson E, Larsson DG.** 2015. Co-occurrence of  
612 resistance genes to antibiotics, biocides and metals reveals novel insights into their co-  
613 selection potential. *BMC Genomics* **16**:964.
- 614 48. **Buffet-Bataillon S, Tattevin P, Bonnaure-Mallet M, Jolivet-Gougeon A.** 2012.  
615 Emergence of resistance to antibacterial agents: the role of quaternary ammonium  
616 compounds--a critical review. *Int J Antimicrob Agents* **39**:381-389.

- 617 49. **Petersen TN, Brunak S, von Heijne G, Nielsen H.** 2011. SignalP 4.0: discriminating  
618 signal peptides from transmembrane regions. *Nat Methods* **8**:785-786.
- 619 50. **Stoczko M, Frere JM, Rossolini GM, Docquier JD.** 2008. Functional diversity among  
620 metallo- $\beta$ -lactamases: characterization of the CAR-1 enzyme of *Erwinia carotovora*.  
621 *Antimicrob Agents Chemother* **52**:2473-2479.
- 622 51. **Docquier JD, Pantanella F, Giuliani F, Thaller MC, Amicosante G, Galleni M, Frere**  
623 **JM, Bush K, Rossolini GM.** 2002. CAU-1, a subclass B3 metallo- $\beta$ -lactamase of low  
624 substrate affinity encoded by an ortholog present in the *Caulobacter crescentus*  
625 chromosome. *Antimicrob Agents Chemother* **46**:1823-1830.
- 626 52. **Galleni M, Lamotte-Brasseur J, Rossolini GM, Spencer J, Dideberg O, Frere JM.**  
627 2001. Standard numbering scheme for class B  $\beta$ -lactamases. *Antimicrob Agents*  
628 *Chemother* **45**:660-663.
- 629 53. **Docquier J-D, Benvenuti M, Calderone V, Stoczko M, Menciassi N, Rossolini GM,**  
630 **Mangani S.** 2010. High-resolution crystal structure of the subclass B3 metallo- $\beta$ -  
631 lactamase BJP-1: rational basis for substrate specificity and interaction with  
632 sulfonamides. *Antimicrob Agents Chemother* **54**:4343-4351.
- 633 54. **Page MI, Badarau A.** 2008. The mechanisms of catalysis by metallo  $\beta$ -lactamases.  
634 *Bioinorg Chem Appl* doi:10.1155/2008/576297:576297.
- 635 55. **Addison AW, Rao TN, Reedijk J, Vanriijn J, Verschoor GC.** 1984. Synthesis,  
636 Structure, and Spectroscopic Properties of Copper(Ii) Compounds Containing Nitrogen  
637 Sulfur Donor Ligands - the Crystal and Molecular-Structure of Aqua[1,7-Bis(N-  
638 Methylbenzimidazol-2'-Yl)-2,6-Dithiaheptane]Copper(Ii) Perchlorate. *Journal of the*  
639 *Chemical Society-Dalton Transactions* doi:Doi 10.1039/Dt9840001349:1349-1356.

- 640 56. **Yamaguchi Y, Takashio N, Wachino J, Yamagata Y, Arakawa Y, Matsuda K,**  
641 **Kurosaki H.** 2010. Structure of metallo- $\beta$ -lactamase IND-7 from a *Chryseobacterium*  
642 *indologenes* clinical isolate at 1.65-Å resolution. *J Biochem* **147**:905-915.
- 643 57. **Wachino J, Yamaguchi Y, Mori S, Kurosaki H, Arakawa Y, Shibayama K.** 2013.  
644 Structural insights into the subclass B3 metallo- $\beta$ -lactamase SMB-1 and the mode of  
645 inhibition by the common metallo- $\beta$ -lactamase inhibitor mercaptoacetate. *Antimicrob*  
646 *Agents Chemother* **57**:101-109.
- 647 58. **Krissinel E, Henrick K.** 2004. Secondary-structure matching (SSM), a new tool for fast  
648 protein structure alignment in three dimensions. *Acta Crystallogr D Biol Crystallogr*  
649 **60**:2256-2268.
- 650 59. **Ullah JH, Walsh TR, Taylor IA, Emery DC, Verma CS, Gamblin SJ, Spencer J.**  
651 1998. The crystal structure of the L1 metallo- $\beta$ -lactamase from *Stenotrophomonas*  
652 *maltophilia* at 1.7 Å resolution. *J Mol Biol* **284**:125-136.
- 653 60. **Garcia-Saez I, Mercuri PS, Papamicael C, Kahn R, Frere JM, Galleni M, Rossolini**  
654 **GM, Dideberg O.** 2003. Three-dimensional structure of FEZ-1, a monomeric subclass  
655 B3 metallo- $\beta$ -lactamase from *Fluoribacter gormanii*, in native form and in complex with  
656 D-captopril. *J Mol Biol* **325**:651-660.
- 657 61. **Leiros HK, Borra PS, Brandsdal BO, Edvardsen KS, Spencer J, Walsh TR,**  
658 **Samuelsen O.** 2012. Crystal structure of the mobile metallo- $\beta$ -lactamase AIM-1 from  
659 *Pseudomonas aeruginosa*: insights into antibiotic binding and the role of Gln157.  
660 *Antimicrob Agents Chemother* **56**:4341-4353.



- 661 62. **Carenbauer AL, Garrity JD, Periyannan G, Yates RB, Crowder MW.** 2002. Probing  
662 substrate binding to Metallo- $\beta$ -Lactamase L1 from *Stenotrophomonas maltophilia* by  
663 using site-directed mutagenesis. BMC Biochem **3**:4.
- 664 63. **Mercuri PS, Garcia-Saez I, De Vriendt K, Thamm I, Devreese B, Van Beeumen J,**  
665 **Dideberg O, Rossolini GM, Frere JM, Galleni M.** 2004. Probing the specificity of the  
666 subclass B3 FEZ-1 metallo- $\beta$ -lactamase by site-directed mutagenesis. J Biol Chem  
667 **279**:33630-33638.
- 668 64. **Garrity JD, Carenbauer AL, Herron LR, Crowder MW.** 2004. Metal binding Asp-  
669 120 in metallo- $\beta$ -lactamase L1 from *Stenotrophomonas maltophilia* plays a crucial role in  
670 catalysis. J Biol Chem **279**:920-927.
- 671 65. **Spencer J, Read J, Sessions RB, Howell S, Blackburn GM, Gamblin SJ.** 2005.  
672 Antibiotic recognition by binuclear metallo- $\beta$ -lactamases revealed by X-ray  
673 crystallography. J Am Chem Soc **127**:14439-14444.
- 674 66. **Crowder MW, Walsh TR, Banovic L, Pettit M, Spencer J.** 1998. Overexpression,  
675 purification, and characterization of the cloned metallo- $\beta$ -lactamase L1 from  
676 *Stenotrophomonas maltophilia*. Antimicrob Agents Chemother **42**:921-926.
- 677 67. **Simm AM, Higgins CS, Carenbauer AL, Crowder MW, Bateson JH, Bennett PM,**  
678 **Clarke AR, Halford SE, Walsh TR.** 2002. Characterization of monomeric L1 metallo- $\beta$ -  
679 -lactamase and the role of the N-terminal extension in negative cooperativity and  
680 antibiotic hydrolysis. J Biol Chem **277**:24744-24752.
- 681 68. **Spencer J, Clarke AR, Walsh TR.** 2001. Novel mechanism of hydrolysis of therapeutic  
682 beta-lactams by *Stenotrophomonas maltophilia* L1 metallo- $\beta$ -lactamase. J Biol Chem  
683 **276**:33638-33644.

- 684 69. **Mercuri PS, Bouillenne F, Boschi L, Lamotte-Brasseur J, Amicosante G, Devreese**  
685 **B, van Beeumen J, Frere JM, Rossolini GM, Galleni M.** 2001. Biochemical  
686 characterization of the FEZ-1 metallo- $\beta$ -lactamase of *Legionella gormanii* ATCC  
687 33297T produced in *Escherichia coli*. *Antimicrob Agents Chemother* **45**:1254-1262.
- 688 70. **Sievers F, Wilm A, Dineen D, Gibson TJ, Karplus K, Li W, Lopez R, McWilliam H,**  
689 **Remmert M, Soding J, Thompson JD, Higgins DG.** 2011. Fast, scalable generation of  
690 high-quality protein multiple sequence alignments using Clustal Omega. *Mol Syst Biol*  
691 **7**:539.
- 692 71. **Kabsch W, Sander C.** 1983. Dictionary of protein secondary structure: pattern  
693 recognition of hydrogen-bonded and geometrical features. *Biopolymers* **22**:2577-2637.
- 694 72. **Robert X, Gouet P.** 2014. Deciphering key features in protein structures with the new  
695 ENDscript server. *Nucleic Acids Res* **42**:W320-324.
- 696 73. **Felsenstein J.** 1989. PHYLIP - Phylogeny Inference Package (Version 3.2). *Cladistics*  
697 **5**:164 - 166.
- 698
- 699

700 **Table 1. Effect of RM3 Expression on  $\beta$ -lactam MICs ( $\mu\text{g} / \text{ml}$ ) for Recombinant**  
 701 ***Escherichia coli* EC100.**

	AMP	AMX	CAR	TMC	ATM	CTX	CAZ	IPM
pCF430 <sup>a</sup>	8	8	32	16	0.25	0.25	0.5	0.5
pCF430:RM3 <sup>b</sup>	16	8	32	32	0.5	0.25	8	1

702

703 <sup>a</sup> MIC values of empty pCF430 in *Escherichia coli* EC100.

704 <sup>b</sup> MIC values for pCF430 carrying 8 kb RM3 metagenomic fragment

705 AMP = ampicillin, AMX = amoxicillin, CAR = carbenicillin, TMC = temocillin, ATM =

706 aztreonam, CTX = Cefotaxime, CAZ = Ceftazidime, IPM = imipenem.

707

708 **Table 2. Kinetic parameters for Hydrolysis of Selected  $\beta$ -Lactams by Rm3 and Selected B3 MBLs.**

$\beta$ -lactam	Rm3			L1			FEZ-1 <sup>d</sup>			BJP-1 <sup>e</sup>			AIM-1 <sup>f</sup>			SMB-1 <sup>g</sup>		
	$K_M^a$	$k_{cat}^b$	$k_{cat}/K_M^c$	$K_M^a$	$k_{cat}^b$	$k_{cat}/K_M^c$	$K_M^a$	$k_{cat}^b$	$k_{cat}/K_M^c$	$K_M^a$	$k_{cat}^b$	$k_{cat}/K_M^c$	$K_M^a$	$k_{cat}^b$	$k_{cat}/K_M^c$	$K_M^a$	$k_{cat}^b$	$k_{cat}/K_M^c$
Penicillin G	ND	ND	4.1 x 10 <sup>4</sup>	75 $\pm 10^*$	410 $\pm 20$	5.5 x 10 <sup>6</sup>	590 $\pm 70$	70 $\pm 5$	1.1 x 10 <sup>5</sup>	130	18	1.3 x 10 <sup>5</sup>	31	778	2.6 x 10 <sup>7</sup>	ND	ND	ND
Ampicillin	1600 $\pm 260$	33.6 $\pm 3$	2.1 x 10 <sup>4</sup>	300 $\pm 15$	580 $\pm 20$	1.9 x 10 <sup>6</sup>	>5000	>5.5	1.1 x 10 <sup>4</sup>	670	13	1.9 x 10 <sup>4</sup>	41	594	1.4 x 10 <sup>6</sup>	102	247	2.4 x 10 <sup>6</sup>
Cefoxitin	ND	ND	1.5 x 10 <sup>4</sup>	3.3 $\pm 0.4^*$	2.2 $\pm 0.1$	6.7 x 10 <sup>5</sup>	11 $\pm 1$	3 $\pm 0.5$	2.7 x 10 <sup>5</sup>	140	10	7.1 x 10 <sup>4</sup>	26	145	5.7 x 10 <sup>6</sup>	26	39	1.5 x 10 <sup>6</sup>
Ceftazidime	ND	ND	2.1 x 10 <sup>4</sup>	145 $\pm 13^{**}$	27 $\pm 3$	2.0 x 10 <sup>5</sup>	>1000	>4	4.0 x 10 <sup>3</sup>	>700	>3	4.3 x 10 <sup>3</sup>	148	7	4.9 x 10 <sup>4</sup>	57	4.4	7.7 x 10 <sup>4</sup>
Cefotaxime	ND	ND	7.1 x 10 <sup>4</sup>	160 $\pm 20^*$	140 $\pm 9$	8.8 x 10 <sup>5</sup>	70 $\pm 8$	165 $\pm 15$	2.4 x 10 <sup>6</sup>	300	41	1.4 x 10 <sup>5</sup>	49	609	1.2 x 10 <sup>7</sup>	35	31	8.9 x 10 <sup>5</sup>
Meropenem	232 $\pm 9$	8.9 $\pm 0.2$	3.8 x 10 <sup>4</sup>	13 ***	77	5.9 x 10 <sup>6</sup>	85 $\pm 3$	45 $\pm 2$	5.0 x 10 <sup>5</sup>	190	156	8.3 x 10 <sup>5</sup>	163	1000	6.8 x 10 <sup>6</sup>	144	604	4.2 x 10 <sup>6</sup>
Imipenem	ND	ND	1.0 x 10 <sup>4</sup>	48 $\pm 8^{**}$	384 $\pm 6$	8 x 10 <sup>6</sup>	>1000	>200	2.0 x 10 <sup>5</sup>	260	15	6.0 x 10 <sup>4</sup>	97	1700	1.7 x 10 <sup>7</sup>	133	518	3.9 x 10 <sup>6</sup>
Aztreonam	NH	ND	ND	ND	ND	ND	>1000	<10 <sup>-2</sup>	<10	NH	ND	ND	NH	ND	ND	NH	ND	ND

 709 <sup>a</sup>  $\mu\text{M}$  <sup>b</sup>  $\text{s}^{-1}$  <sup>c</sup>  $\text{M}^{-1} \text{s}^{-1}$ 

710 Kinetic data for L1 are from (66)\*, (67)\*\*, (68)\*\*\*.

711 Kinetic data for other enzymes are from FEZ-1 (69), BJP-1 (26), AIM-1 (14) and SMB-1 (15).

712

713

714 **Table 3. Crystallographic Data Collection and Refinement Statistics**

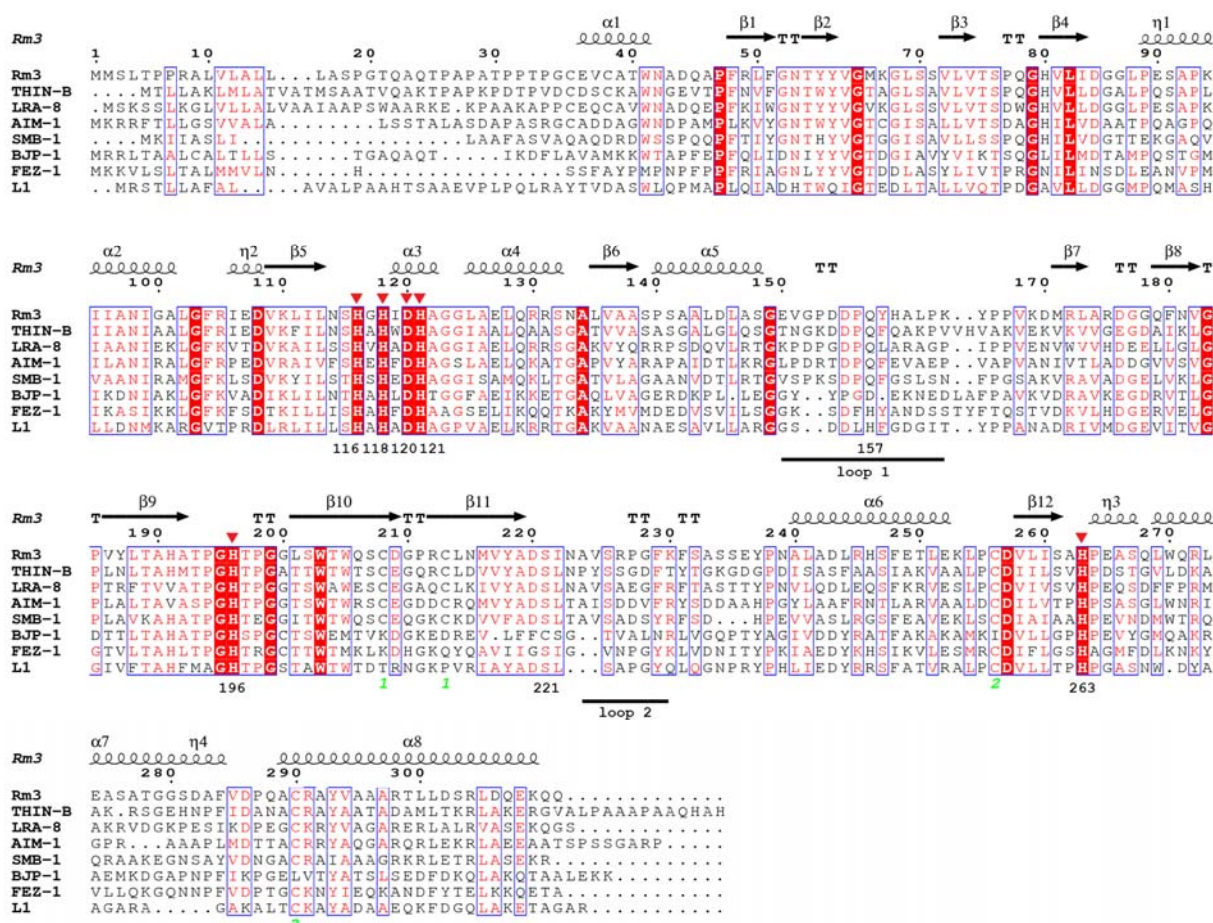
<b>Data Collection</b>	
Beamline	DLS (I04)
Wavelength (Å)	0.9795
Space Group	P2 <sub>1</sub>
Cell Dimensions	
<i>a</i> , <i>b</i> , <i>c</i> (Å)	45.88, 74.45, 77.46
$\alpha$ , $\beta$ , $\gamma$	90, 99.48, 90
Molecules/asymmetric unit	2
Resolution (Å)	53.32 - 1.75 (1.78 – 1.75) <sup>a</sup>
No. of unique reflections	50630 (2761) <sup>a</sup>
Redundancy	2.4 (2.3) <sup>a</sup>
<i>R</i> <sub>merge</sub>	0.055 (0.363) <sup>a</sup>
<i>CC1/2</i>	0.997 (0.821) <sup>a</sup>
<i>I</i> / $\sigma$	9.1 (2.1) <sup>a</sup>
Completeness (%)	97.6 (97.2) <sup>a</sup>
<b>Refinement</b>	
Resolution (Å)	53.32 - 1.75 (1.78 – 1.75) <sup>a</sup>
No. of reflections	50593 (2780) <sup>a</sup>
<i>R</i> <sub>work</sub> / <i>R</i> <sub>free</sub> <sup>b</sup>	20.28 / 22.94 (31.15 / 32.18) <sup>a</sup>
No. Protein atoms	2022 <sup>c</sup> / 2029 <sup>d</sup>
No. Zinc ions	7
No. Water molecules	302
B factors (protein)	25.58 <sup>c</sup> / 26.65 <sup>d</sup>
B-factor (zinc)	19.38
B-factor (water)	29.25
Bond length rmsd (Å)	0.007
Bond angle rmsd (°)	1.09

715 <sup>a</sup>Highest resolution shell statistics are shown in parentheses.716 <sup>b</sup>*R*<sub>free</sub> was calculated with 5% of reflections omitted from refinement717 <sup>c</sup>chain A718 <sup>d</sup>chain B

## Characterization of Rm3 Metallo- $\beta$ -Lactamase

719 **Figure 1: Sequence Alignment of SubClass B3 Metallo- $\beta$ -Lactamases.** Alignment of selected  
 720 subclass B3 MBLs. Sequences were aligned using ClustalOmega (70) invariant residues are  
 721 highlighted with a red background, conservative substitutions are in red text. Residue numbering  
 722 is according to the BBL standard numbering scheme (52); discontinuities (e.g. between residues  
 723 5- 70 , 80 – 90 and 150 – 170) are due to omission from the Figure of other MBL subclasses.  
 724 Secondary structure assignments (DSSP; (71)) are from Rm3 structure (this work). Zinc binding  
 725 residues are indicated by red triangles. Cysteine pairs 208 and 213, and 256 and 290 are labeled  
 726 1 and 2, respectively. Positions of key Rm3 residues and of Rm3 loops 1 and 2 are labeled below  
 727 the alignment. This Figure was prepared using EsPrint (72).

728



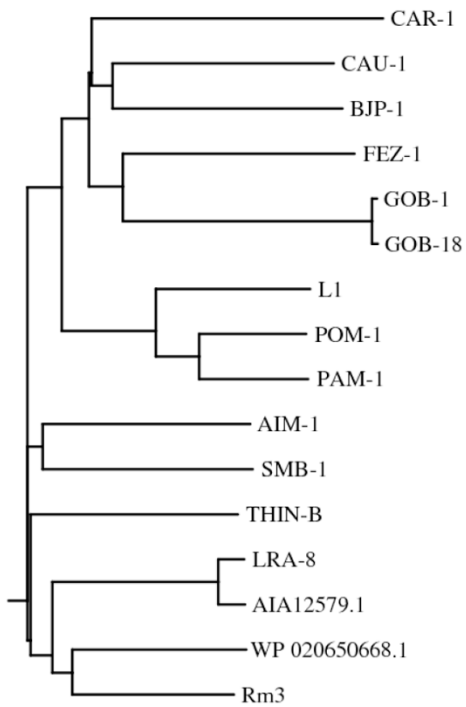
729

730

Characterization of Rm3 Metallo- $\beta$ -Lactamase

731 **Figure 2: Phylogenetic Tree of Selected Subclass B3 Metallo- $\beta$ -Lactamases.** Sequences were  
732 aligned using ClustalOmega (70) and the phylogenetic tree was visualized using the Drawgram  
733 3.67 component of the PHYLIP package (73).

734

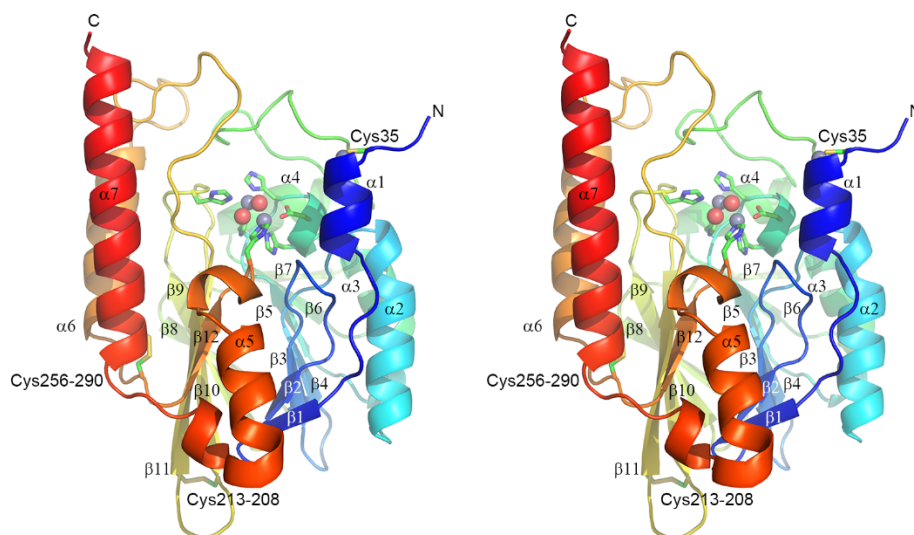


735

736

737 **Figure 3: Overall Structure of Rm3.** Stereo view of Rm3, with protein backbone color-ramped  
738 from blue (N-) to red (C-terminus). Active site residues and disulfide bonds are rendered as  
739 sticks (carbon atoms in green, other atom colors as standard). Zinc ions (gray) and water  
740 molecules (red) are shown as spheres. This Figure was generated using Pymol ([www.pymol.org](http://www.pymol.org)).

741



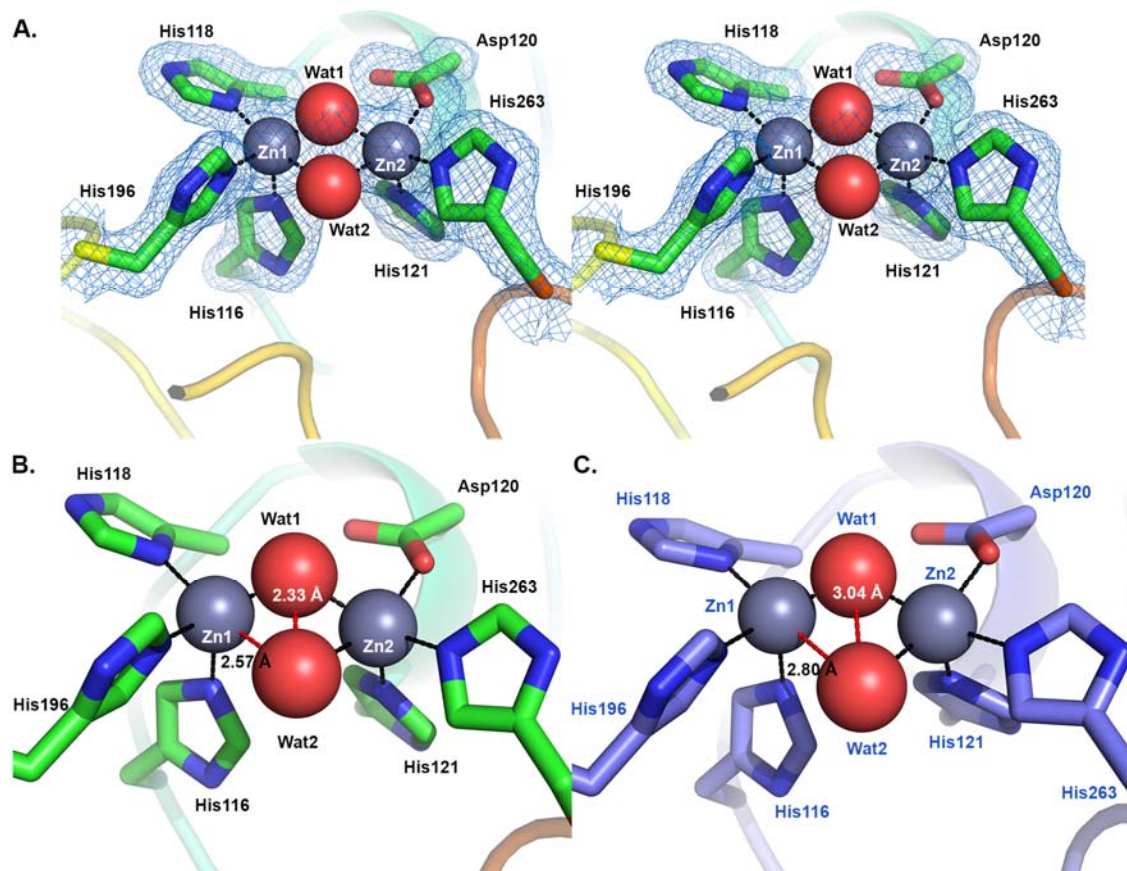
742

743



744 **Figure 4: Rm3 Active Site.** A. Stereoview; carbon atoms are colored green, zinc ions gray,  
 745 water molecules red, other colors as standard. Electron density map is  $2|F_o| - |F_c| \cdot \phi_{calc}$ , contoured  
 746 at  $1.5 \sigma$ . B. Active site of Rm3 showing position of Wat2 relative to Zn1 (distance in black) and  
 747 Wat1 (distance in white). C. Active site of L1 (pdb 1SML, (59)) showing position of Wat2  
 748 relative to Zn1 and Wat1. This Figure was generated using Pymol.

749

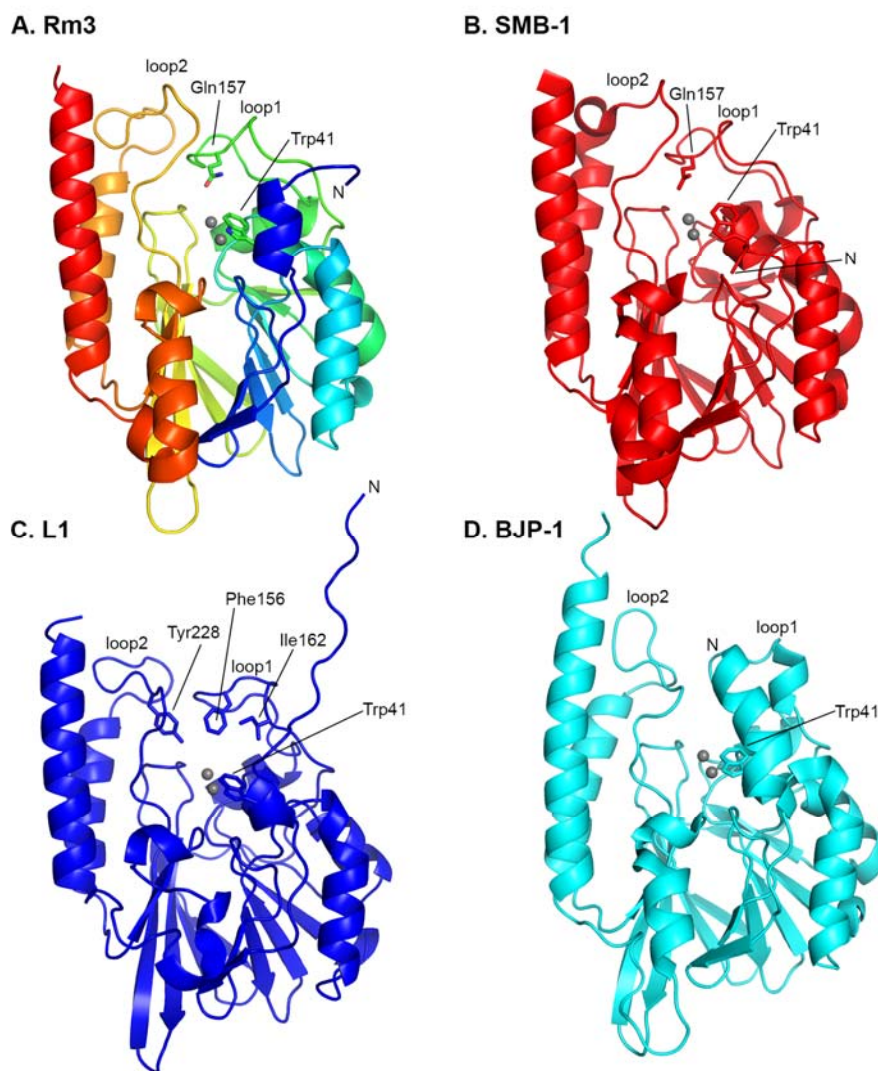


750

751

752 **Figure 5. Comparison of Rm3 with Other B3 MBLs.** Superposition of Rm3 structure upon  
753 those of other B3 MBLs. A. Overall fold of Rm3 (chain A; color-ramped from N- (blue) to C-  
754 (red) terminus. B. SMB-1 (pdb 3VPE (57)). C. L1 (pdb 1SML (59)). D. BJP-1 (pdb 3LVZ (53)).  
755 Residues discussed in the text are rendered as sticks. This Figure was generated using Pymol.

756

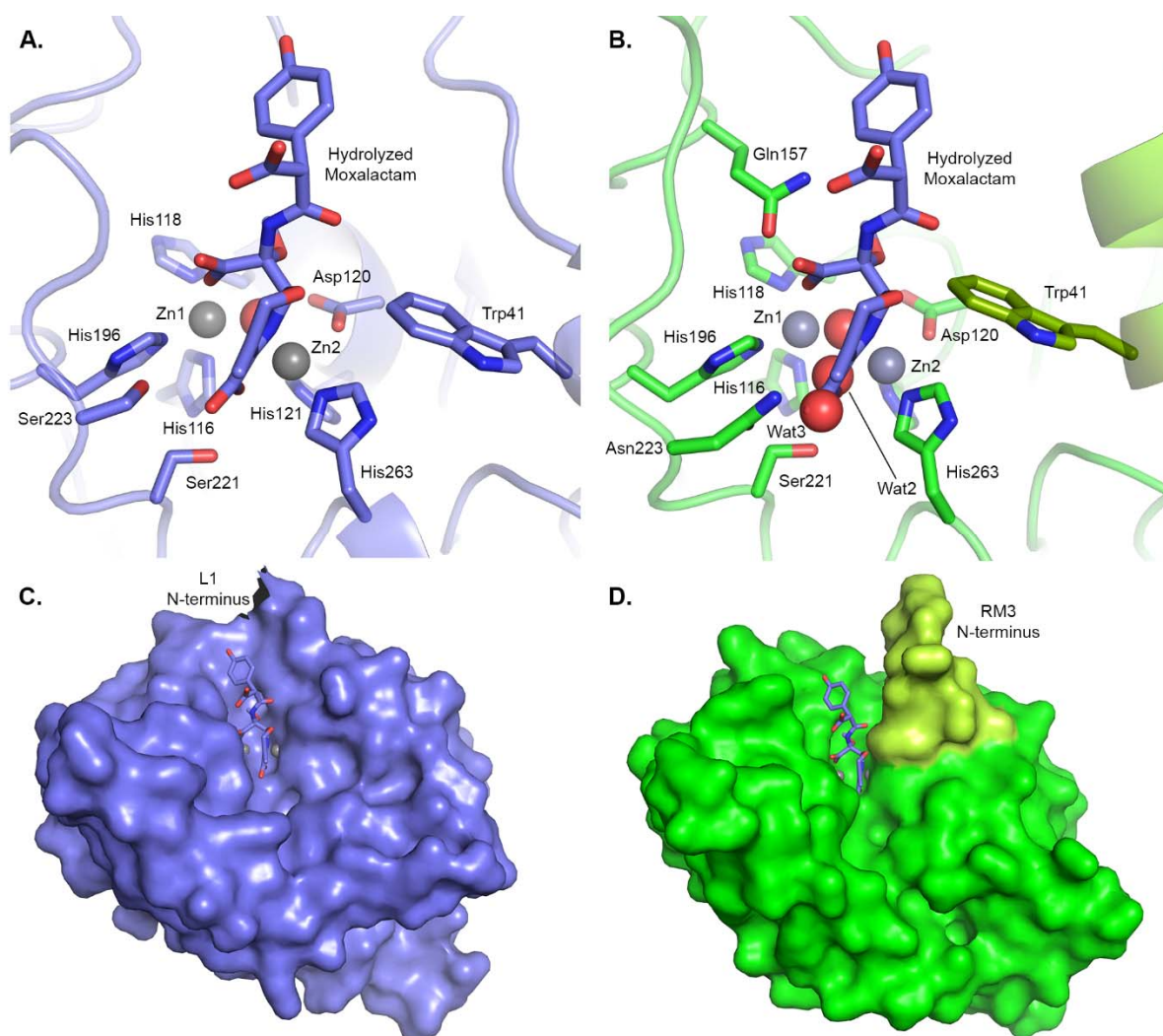


757

758

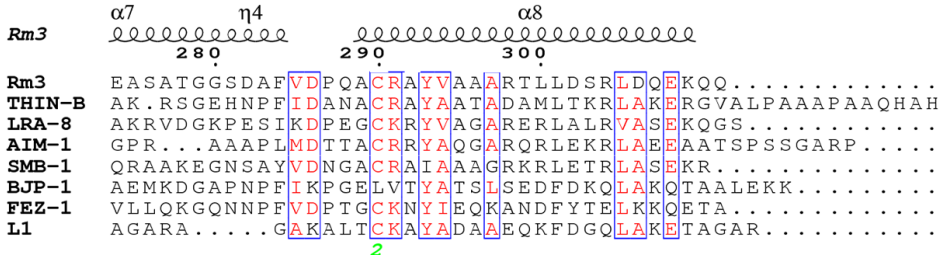
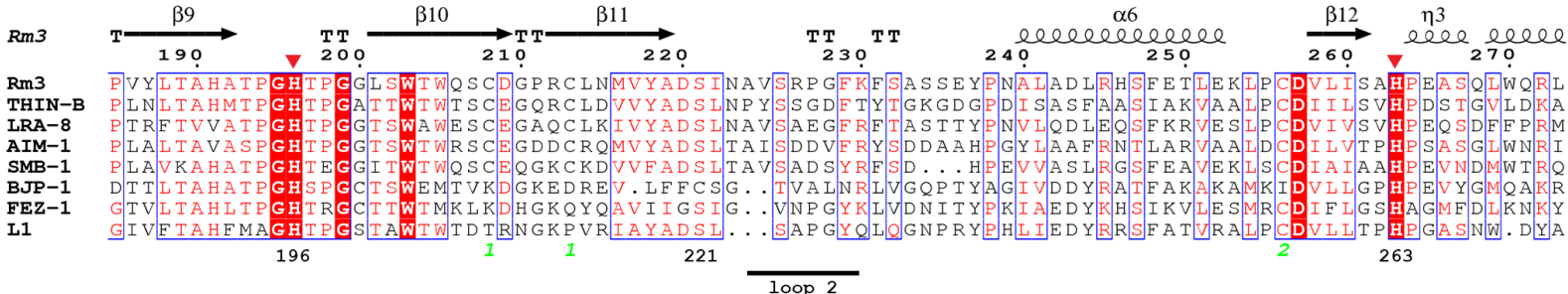
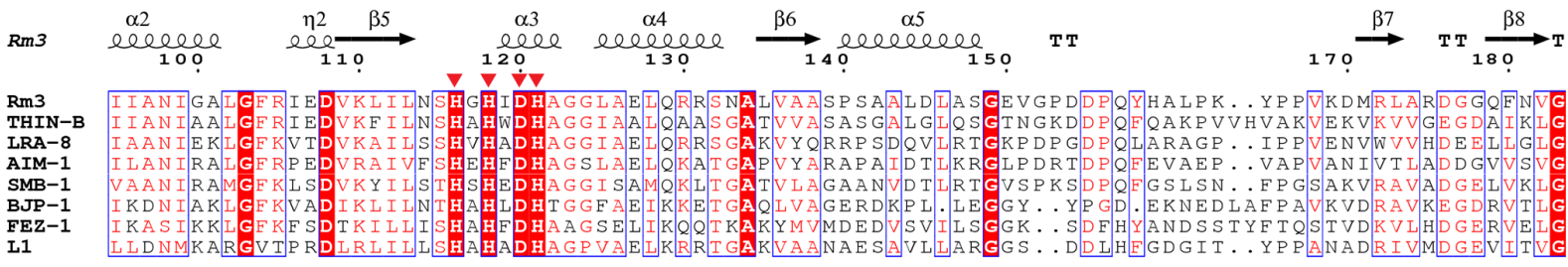
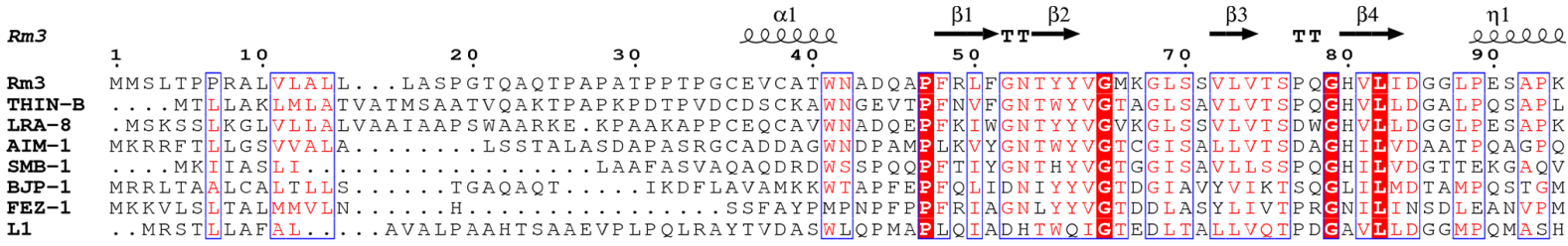
759 **Figure 6: Proposed Interactions of Rm3 with Substrates.** A. Crystal structure of L1 bound to  
 760 hydrolyzed moxalactam (pdb 2AIO; (65)). B. Superposition of hydrolyzed moxalactam from pdb  
 761 2AIO on structure of Rm3 (this work). Note that superposition places the moxalactam C4  
 762 carboxylate over Wat2 and Wat3, N5 and the C4 carboxylate in proximity to Zn2 and the C8  
 763 carboxylate close to Zn1. C. and D. space-filling representations of the L1 complex (pdb 2AIO)  
 764 and Rm3 structure (this work) with bound moxalactam superposed in stick form. The extended  
 765 N-terminus of Rm3 (residues 32 - 43) is highlighted in pale green. This Figure was generated  
 766 using Pymol.

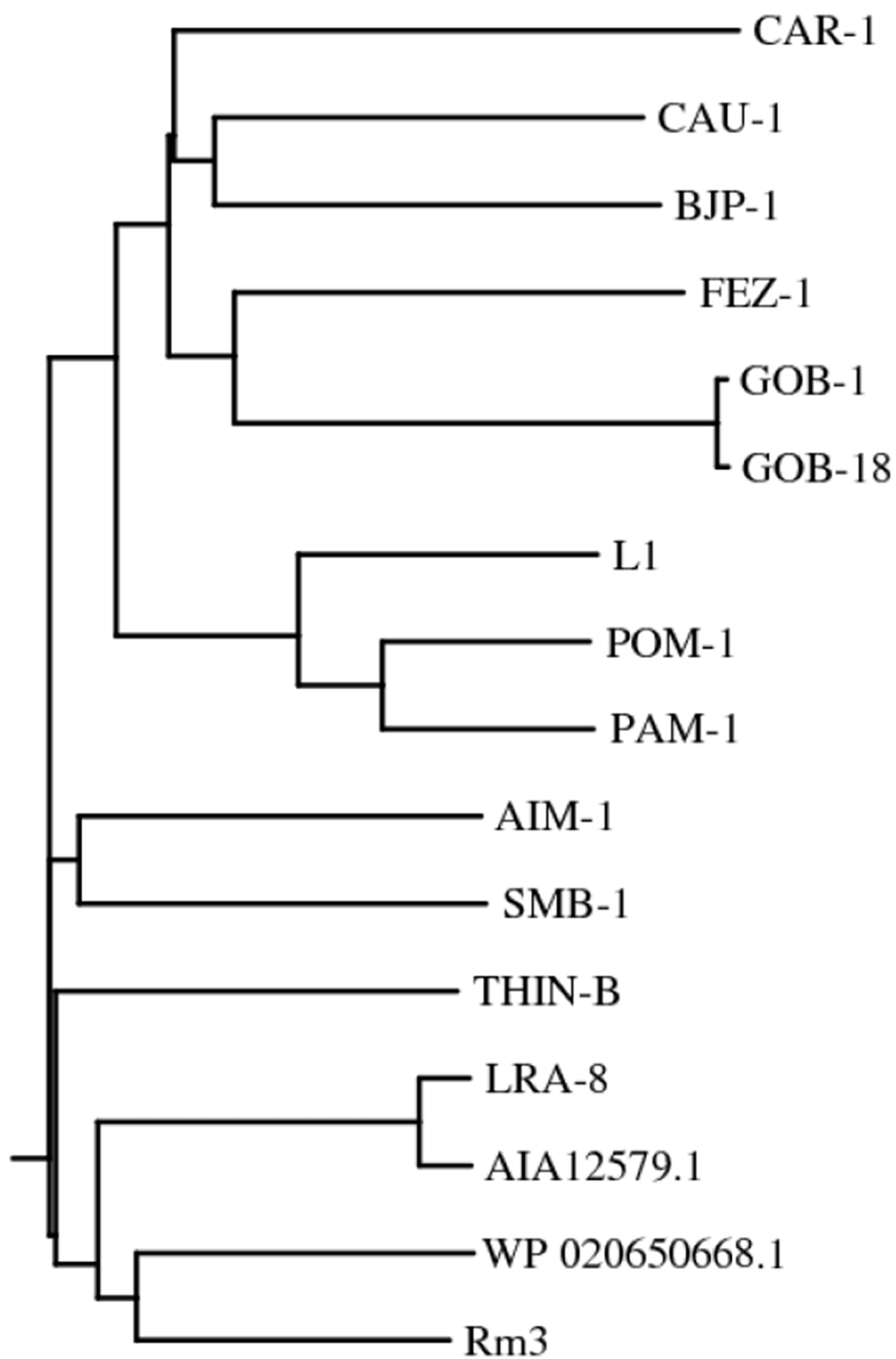
767

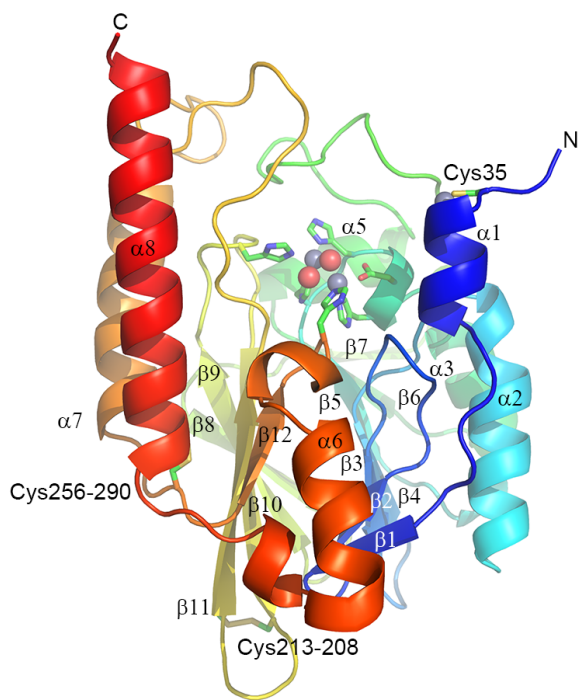
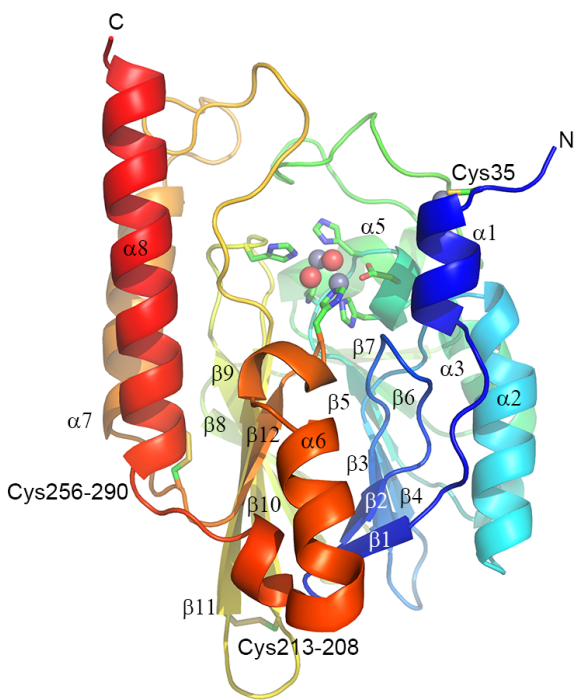


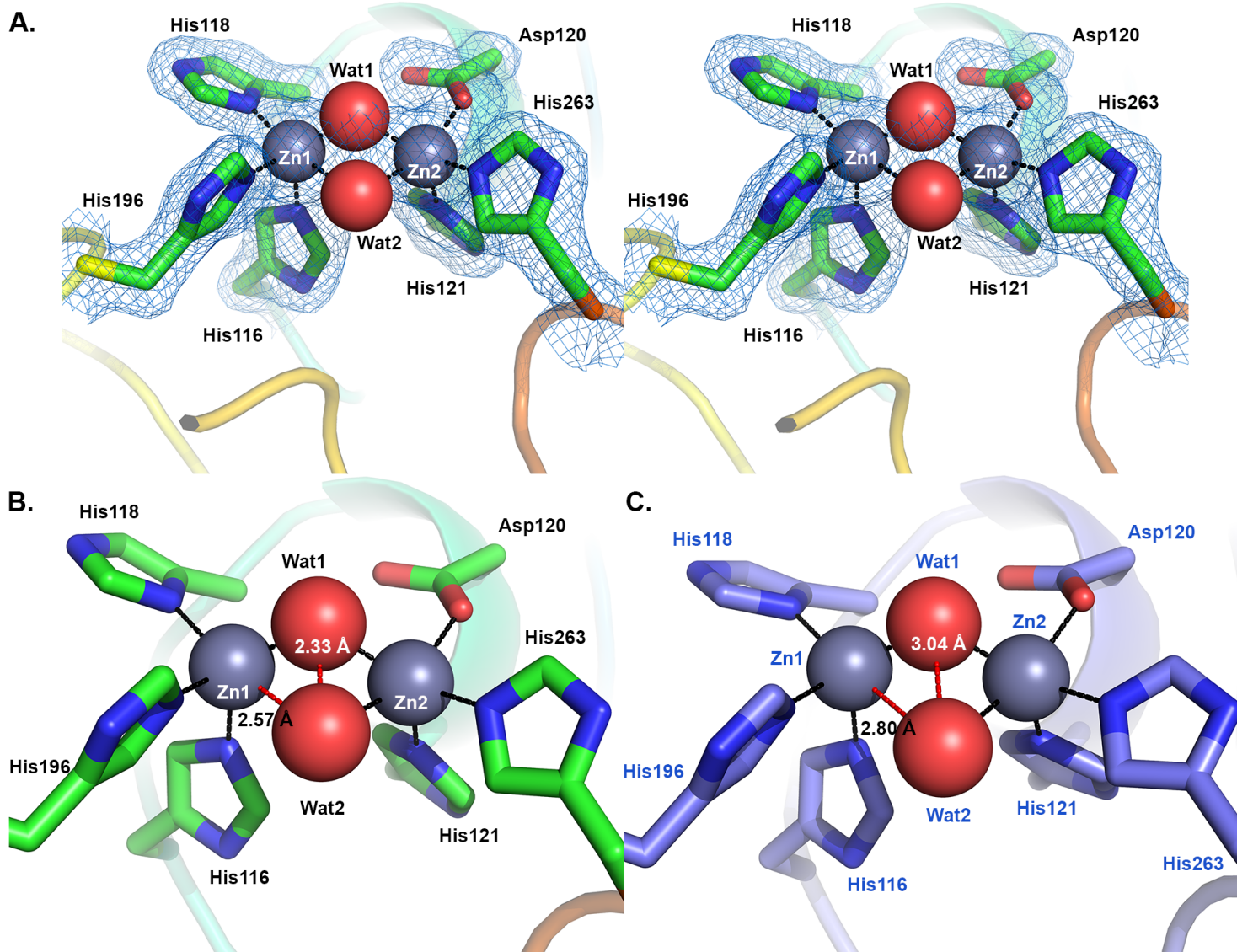
768

769

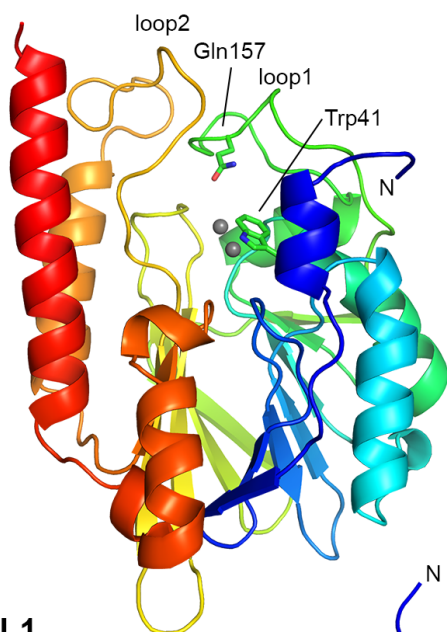




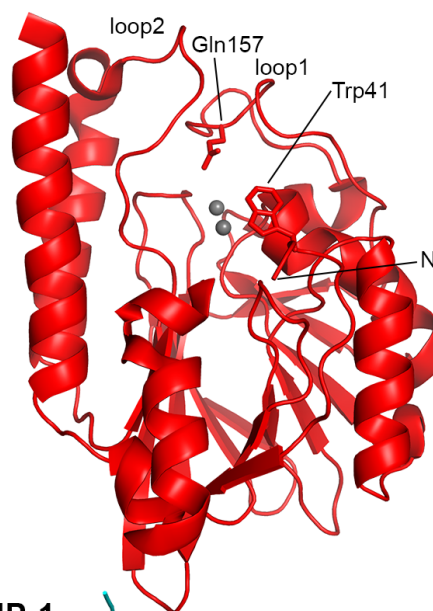




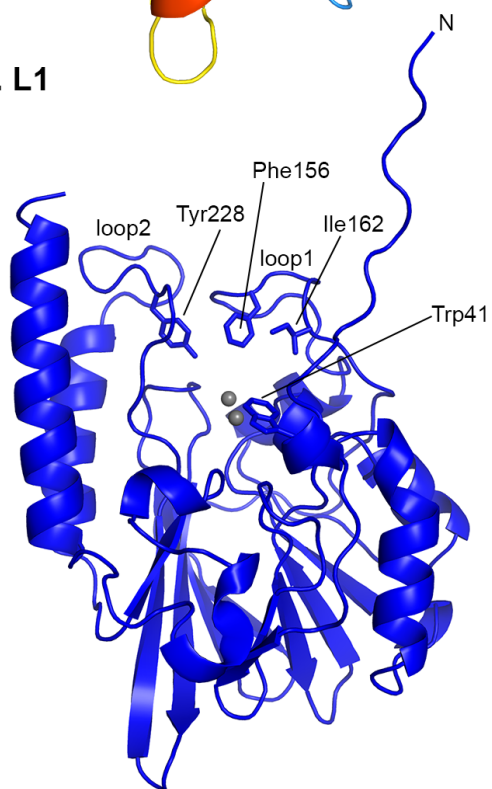
**A. Rm3**



**B. SMB-1**



**C. L1**



**D. BJP-1**

